Zebrafish SPI-1 (PU.1) Marks a Site of Myeloid Development Independent of Primitive Erythropoiesis: Implications for Axial Patterning

Graham J. Lieschke,*,[1],[3] **Andrew C. Oates,**†,[1],[2] **Barry H. Paw,**‡
Margaret A. Thompson,‡ **Nathan E. Hall,*** **Alister C. Ward,***
Robert K. Ho,†,[2] **Leonard I. Zon,**‡ **and Judith E. Layton***

**Ludwig Institute for Cancer Research, The Royal Melbourne Hospital, Parkville, Victoria,
3050, Australia;* †*Department of Molecular Biology, Princeton University, Princeton,
New Jersey 08544; and* ‡*Howard Hughes Medical Institute, Childrens Hospital,
300 Longwood Avenue, Boston, Massachusetts 02115*

The mammalian transcription factor SPI-1 (synonyms: SPI1, PU.1, or Sfpi1) plays a critical role in myeloid development. To examine early myeloid commitment in the zebrafish embryo, we isolated a gene from zebrafish that is a *SPI-1* orthologue on the basis of homology and phylogenetic considerations. The zebrafish *spi1* (*pu1*) gene was first expressed at 12 h postfertilization in rostral lateral plate mesoderm (LPM), anatomically isolated from erythroid development in caudal lateral plate mesoderm. Fate-mapping traced rostral LPM cells from the region of initial *spi1* expression to a myeloid fate. *spi1* expression was lost in the bloodless mutant *cloche*, but rostral *spi1* expression and myeloid development were preserved in the mutant *spadetail*, despite its complete erythropoietic failure. This dissociation of myeloid and erythroid development was further explored in studies of embryos overexpressing BMP-4, or chordin, in *bmp*-deficient *swirl* and *snailhouse* mutants, and *chordin*-deficient *chordino* mutants. These studies demonstrate that, in zebrafish, *spi1* marks a rostral population of LPM cells committed to a myeloid fate anatomically separated from and developmentally independent of erythroid commitment in the caudal LPM. Such complete anatomical and developmental dissociation of two hematopoietic lineages adds an interesting complexity to the understanding of vertebrate hematopoietic development and presents significant implications for the mechanisms regulating axial patterning.   © 2002 Elsevier Science (USA)

Key Words: Danio rerio; hematopoiesis; myelopoiesis; lateral plate mesoderm; SPI-1; PU.1; bone morphogenetic protein (BMP).

INTRODUCTION

The zebrafish (*Danio rerio*) has proven to be a versatile and informative model for the study of early hematopoietic commitment (reviewed in Amatruda and Zon, 1999). Zebrafish orthologues have been isolated for a range of molecules important in mammalian hematopoietic commitment, suggesting that, in zebrafish, embryonic and definitive hematopoiesis depends on similar molecular mechanisms and genetic controls to that of mammals.

Zebrafish hematopoietic genes isolated by various strategies include the transcription factors *scl*, *lmo2*, *gata1*, *gata2*, *cmyb*, *runx* family members and *cbfb* (Liao *et al.,* 1998; Gering *et al.,* 1998; Thompson *et al.,* 1998; Detrich *et al.,* 1995; Kataoka *et al.,* 2000; Blake *et al.,* 2000), some erythroid lineage-specific genes, including the *globin* gene family and *β-spectrin* (Chan *et al.,* 1997; Liao *et al.,* 2000a), the heme-synthesis genes δ-*aminolevulinate synthetase*, *uroporphyrinogen decarboxylase*, and *ferrochelatase* (Brownlie *et al.,* 1998; Wang *et al.,* 1998; Childs *et al.,* 2000), and intracellular signaling molecules of the JAK and STAT families (Conway *et al.,* 1997; Oates *et al.,* 1999a,b). The optical transparency of young zebrafish embryos means that endogenous red hemoglobin pigment serves well as a visual flag for both the location and the adequacy of erythropoiesis, and based on this visual tag of hematopoi-

[1] These authors contributed equally to this work.

[2] Present address: Department of Organismal Biology and Anatomy, University of Chicago, Chicago, IL, 60637.

[3] To whom correspondence should be addressed. Fax: +61-3-9341-3104. E-mail: Graham.Lieschke@ludwig.edu.au.

esis, several large-scale screens for organ-specific zebrafish mutants collected a group of anemic mutants (Ransom *et al.,* 1996; Weinstein *et al.,* 1996). Identification of the mutated genes underpinning these mutant phenotypes has, in some cases, implicated new genes in the erythropoietic process (e.g., *ferroportin1*) (Donovan *et al.,* 2000).

Fate mapping experiments show that primitive circulating blood arises from cells in the radially symmetric zebrafish gastrula that are situated opposite the future embryonic organizer, or shield, which gives rise to the notochord (Kimmel *et al.,* 1990; Warga and Nusslein-Volhard, 1999). Recognizable erythroid blood precursors are first found in the caudal lateral plate mesoderm (LPM; Al-Adhami and Kunz, 1977), which is ventrally located in the body plan of the segmentation-stage embryo. Since the notochord is dorsally located in the embryo, the axis running through the shield and blood-forming region in the gastrula is thought to define the future dorsoventral axis of the zebrafish body plan (Kimmel *et al.,* 1990). Like other vertebrates, zebrafish are viewed as patterning mesoderm along this axis by a gradient of bone morphogenetic protein (BMP) signaling, with highest levels at the blood-forming side of the early embryo (ventral end of the axis), and an active repression of BMP signaling required for the organizer and somitic fates (dorsal end of axis) to develop (Jones *et al.,* 1992; Dale *et al.,* 1992; Piccolo *et al.,* 1996; Neave *et al.,* 1997; Nikaido *et al.,* 1997). Thus, high levels of BMP signaling in the pregastrula demarcate an area of mesoderm opposite the future shield that is committed to form embryonic blood (reviewed in Amatruda and Zon, 1999). The fate of this region of erythroid hematopoietic commitment is elegantly displayed in zebrafish by the restriction of *gata1* expression to the caudal LPM during somitogenesis. As somitogenesis proceeds, these bilateral bands of *gata1*-expressing cells move to the midline in a rostral to caudal wave to form the intermediate cell mass (ICM), an axial mesodermal element ventral to the hypochord (Detrich *et al.,* 1995). As the vasculature condenses in the ICM around these *gata1*-expressing cells, they and their progeny enter the newly established circulation and constitute the primitive wave of erythrocytes.

In contrast to this quite detailed knowledge about zebrafish erythropoiesis, myelopoiesis has been less well characterized in zebrafish. Zebrafish myeloid cells include macrophages and granulocytes (Lieschke *et al.,* 2001; Bennett *et al.,* 2001), which function as the early immune response to bacterial infection, as well as removing cellular debris. At a molecular level, only a few myeloid lineage-specific zebrafish genes have been isolated to date. These include *cfms* and *l-plastin* pertaining to macrophages (Herbomel *et al.,* 1999; Parichy *et al.,* 2000), and *mpo/mpx* and *c/ebp1* pertaining to granulocytes (Lieschke *et al.,* 2001; Bennett *et al.,* 2001; Lyons *et al.,* 2001). Additionally, *ikaros*, *rag1*, and *rag2* orthologues, which mark lymphopoiesis, have also been identified (Haire *et al.,* 2000; Willett *et al.,* 1997).

We now report a comprehensive analysis of early myeloid specification in the zebrafish based on the zebrafish *spi1* gene. SPI-1 (also known as SPI1, Sgfi1, and PU.1) is a member of the E26 transformation-specific (Ets) family of transcription factors that also includes SPI-B and SPI-C proteins (Sharrocks *et al.,* 1997). Spi family members are characterized by a carboxyl-terminal domain that binds to DNA sequences 5′-GAGGAA-3′ (PU box). SPI-1 also contains an N-terminal transactivation domain, and a central PEST domain involved in protein–protein interactions (Pongubala *et al.,* 1993; Klemsz and Maki, 1996). SPI-1 plays a critical role in mammalian myelopoiesis, evidenced by the quantitative and functional deficiencies in macrophages, granulocytes, and lymphocytes manifest in Spi-1-deficient mice immediately after birth (Scott *et al.,* 1994; McKercher *et al.,* 1996). Recently, it has been shown that Spi-1 directly interacts with Gata-1, and mis-expression studies in *Xenopus* demonstrate that a potential consequence of this interaction can be to divert the fate of a Gata-1-expressing cell away from an erythroid fate (Rekhtman *et al.,* 1999; Zhang *et al.,* 2000). *Spi* family members are found in the genomes of agnathans, gnathostomes, reptiles, amphibians, and birds, as well as mammals, suggesting that their functional role is widely conserved (Shintani *et al.,* 2000; Anderson *et al.,* 2001).

In zebrafish, videomicroscopic examination has revealed a mobile population of phagocytes emanating from a region of LPM rostral to the heart (Herbomel *et al.,* 1999). This population of macrophages expressed a zebrafish *l-plastin*, and a novel gene *draculin*, isolated by pattern recognition in a screen of EST expression patterns. Despite their appearance at a rostral postgastrulation site, fate-mapping by early blastomere labeling suggested that these macrophages arise from the ventral end of the presumed dorsoventral axis of the gastrula, consistent with a common origin for erythroid and myeloid cells (Herbomel *et al.,* 1999). Recently, however, several observations across a range of species have challenged the view that a hematopoietic fate results exclusively from the cells located in the region of the gastrula opposite the organizer (Lane and Smith, 1999; Miyanaga *et al.,* 1998; Ohinata *et al.,* 1990; Tracey *et al.,* 1998; and reviewed in Shepard and Zon, 2000).

We were interested in better understanding the molecular basis of myeloid specification in the zebrafish embryo, and here we demonstrate the isolation of zebrafish *spi1*, a *SPI-1* orthologue, providing us with a marker of myeloid development, as shown by fate-mapping *spi1*-expressing cells. Zebrafish *spi1* was expressed in rostral LPM at a site where lineage-specific transcriptionally regulated hematopoietic specification had not previously been demonstrated. We show that both erythrocytes and myeloid cells are lost in *cloche* mutant embryos, whereas there is a selective loss of erythrocytes in the *spadetail* mutant line. We explored the effects of increasing and decreasing effective BMP signaling on myeloid, as distinct from erythroid development, by overexpressing BMPs and their antagonists, and by examining these lineages in loss-of-function mutants in BMP signaling genes. Our results indicate that myeloid and

erythroid development respond differently to these manipulations, a finding at odds with a common origin for these blood lineages. Collectively, these data demonstrate the dissociability of early myeloid and erythroid development in the zebrafish embryo, and lead us to hypothesize a pregastrulation origin for early myeloid cells separate from and closer to the organizer than that for erythrocytes. These studies thus contribute to the evidence mandating a revision of previous models of vertebrate hematopoietic development which postulate that all hematopoietic lineages originate from the same region of the gastrula, to one in which blood arises from multiple locations around the mesodermal margin.

MATERIALS AND METHODS

Zebrafish

Wild-type zebrafish stocks were obtained from a local pet shop and held in the Ludwig Institute for Cancer Research Aquarium Facility employing standard husbandry practices. The *m39 cloche* allele (thought to be a gene deletion; Liao *et al.,* 2000b) and the null *b104 spadetail* allele (Kimmel *et al.,* 1989; Griffin *et al.,* 1998) were used. The *din^{tm84}* and *swirl* (*swr^{ta72}*) alleles of *chordin* and *bmp2b* were used, both of which result in a morphologically unambiguous phenotype at bud stage (Mullins *et al.,* 1996; Hammerschmidt *et al.,* 1996a,b; Schulte-Merker *et al.,* 1997; Kishimoto *et al.,* 1997). The *snh^{ty68}* allele of *snailhouse*, a point mutation in the prodomain of the *bmp7* locus, was used (Dick *et al.,* 2000).

Embryos for developmental studies were collected from tanks and held at 28°C on a plate warmer. Some embryos were raised in egg water supplemented by 0.003% 1-phenyl-2-thiourea (PTU) (Sigma, P-7629) from 12 h postfertilization (hpf) to suppress melanization (e.g., for *in situ* hybridization analysis). In describing zebrafish embryos, we have followed the conventions for terms of direction as recently suggested (Moorman, 2001).

Cloning a Zebrafish spi1 Orthologue

Degenerate oligonucleotide primers corresponding to conserved regions of human and mouse Pu.1 protein were synthesized: WWVDKD/5′-ggggaattcTGGTGGGTNGAYAARGA-3′ and YGK-TGE/5′-cgcggatccTCNCCNGTYTTNCCRTA-3′; underlined lower case sequences correspond to introduced *Eco*RI and *Bam*HI sites, respectively. Total RNA was isolated from either kidneys of adult zebrafish previously treated with phenylhydrazine or zebrafish embryos at 30 hpf. cDNA was synthesized with oligo(dT) primer from total RNA isolated by using standard conditions. PCR amplification was performed with degenerate primers under the following conditions: 94°C for 1 min, 40°C for 1.5 min, 72°C for 1.5 min, for a total of 40 cycles. The predicted ~170-bp fragment was gel-purified, subcloned, and sequenced to confirm its identity. The zebrafish *spi1* cDNA fragment was subsequently used as probe to screen a randomly primed cDNA library derived from wild-type zebrafish kidney. After screening approximately 10^6 plaque forming units of the cDNA library made in the λ ZAP express vector, several positive clones were isolated by serial selection under high-stringency conditions (0.1× SSC and 0.1% SDS at 65°C). A clone derived from the oligo(dT)-primed kidney cDNA was isolated by using the random cDNA clone as probe. The cDNA insert in this clone (pBKCMV*spi1*) was sequenced.

The zebrafish gene represented by this cDNA was named *spi1* in accordance with the Zebrafish Nomenclature Guidelines (http://zfin.org/zf_info/nomen.html) and was approved by the Zebrafish Nomenclature Committee. Acknowledging common usage of the alternate name PU.1 for the mammalian orthologue, its alias as *pu1*, is acknowledged in Genbank and zebrafish databases.

Phylogenetic Analysis

Sequence identity values for the whole molecule and subdomains were determined by using the CLUSTAL algorithm in MegAlign application of the DNASTAR suite of programs (Madison, WI; http://www.dnastar.com) with PAM250 residue weight tables and no manual adjustments. The dendrogram was constructed based on an alignment generated from CLUSTAL X (1.81) (Thompson *et al.,* 1997) using default settings and viewed with TREEVIEW using human ELF5 as an outgroup. Bootstrap values derive from 1000 bootstrap trials.

### Linkage Group Assignment and Synteny Analysis

Linkage group assignment on the LN54 and T51 radiation hybrid panels was achieved by using primers directed to the 3′ UTR of the *spi1* cDNA: 5′-TCAAATGAAAAGCAGCGTCATATTC-3′ and 5′-CCATAGCACATCATGAAAGTTCAC-3′. PCR amplification conditions are as follows: 55°C annealing for 1 min, 72°C elongation for 2 min, and 94°C denaturing for 1 min, for a total of 45 cycles. The synteny analysis was performed by using the consolidated zebrafish maps available from ZFIN (http://zfin.org/ZFIN/) and data available from LocusLink (http://www.ncbi.nlm.nih.gov/LocusLink/).

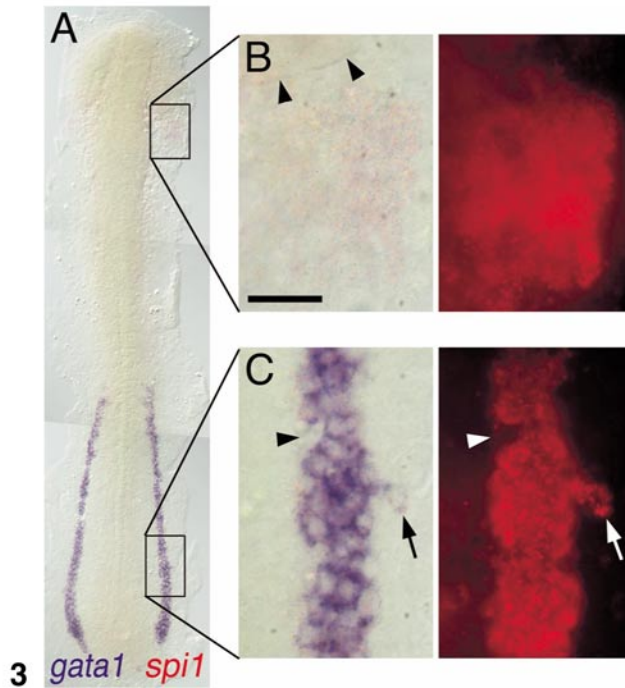### Whole-Mount in Situ Hybridization Gene Expression Analysis

Whole mount *in situ* hybridization analyses were performed as described (Schulte-Merker *et al.,* 1992; Liao *et al.,* 1998; Thompson *et al.,* 1998) by using a hybridization temperature of 70°C. Two-color *in situ* was performed according to Hauptmann and Gerster (1994) and Prince *et al.* (1998), with the exception of the Fast Red prestain washes that used 0.1 M Tris–HCl, pH 8.0. pBKCMV*spi1* was used to generate digoxigenin- and fluorescein-labeled *spi1* riboprobes. To generate a template plasmid for riboprobes corresponding to the first 367 nucleotides of *spi1*, the *Eco*RI–*Stu*1 fragment of pBKCMV*spi1* was subcloned into the *Eco*RI–*Sma*1 site of pBKCMV. Both full-length and short *spi1* antisense riboprobes were transcribed by using T7 polymerase and cDNA templates linearized with *Eco*RI. Sense riboprobes were transcribed with T3 polymerase from templates linearized with either *Xho*I (full-length) or *Kpn*I (short). Controls with sense riboprobes were prepared in parallel with initial *spi1* antisense *in situ* hybridization analyses and showed no staining, hence subsequently they were not routinely repeated. Probes to *gata1*, *scl*, *fli1*, and *nkx2.5* were prepared as previously described (Detrich *et al.,* 1995; Liao *et al.,* 1998; Thompson *et al.,* 1998; Alexander *et al.,* 1998). The blue NBT precipitate sometimes completely quenched the visual and fluorescent signals from the fast-red precipitate, regardless of which way they were deployed in the detection step, and careful adjustment of the staining conditions was required. The false-color images of Fig. 8 were taken in black on white on a CoolSNAP HQ Camera (Roper Scientific Photometrics, Trenton, NJ) by using RS Image 1.7.3 software (Roper Scientific) and a fluorescence equipped Leica FL-III dissecting microscope. The blue dye was imaged utilizing epi-illumination. The Leica FL-III green excitation filter set was used
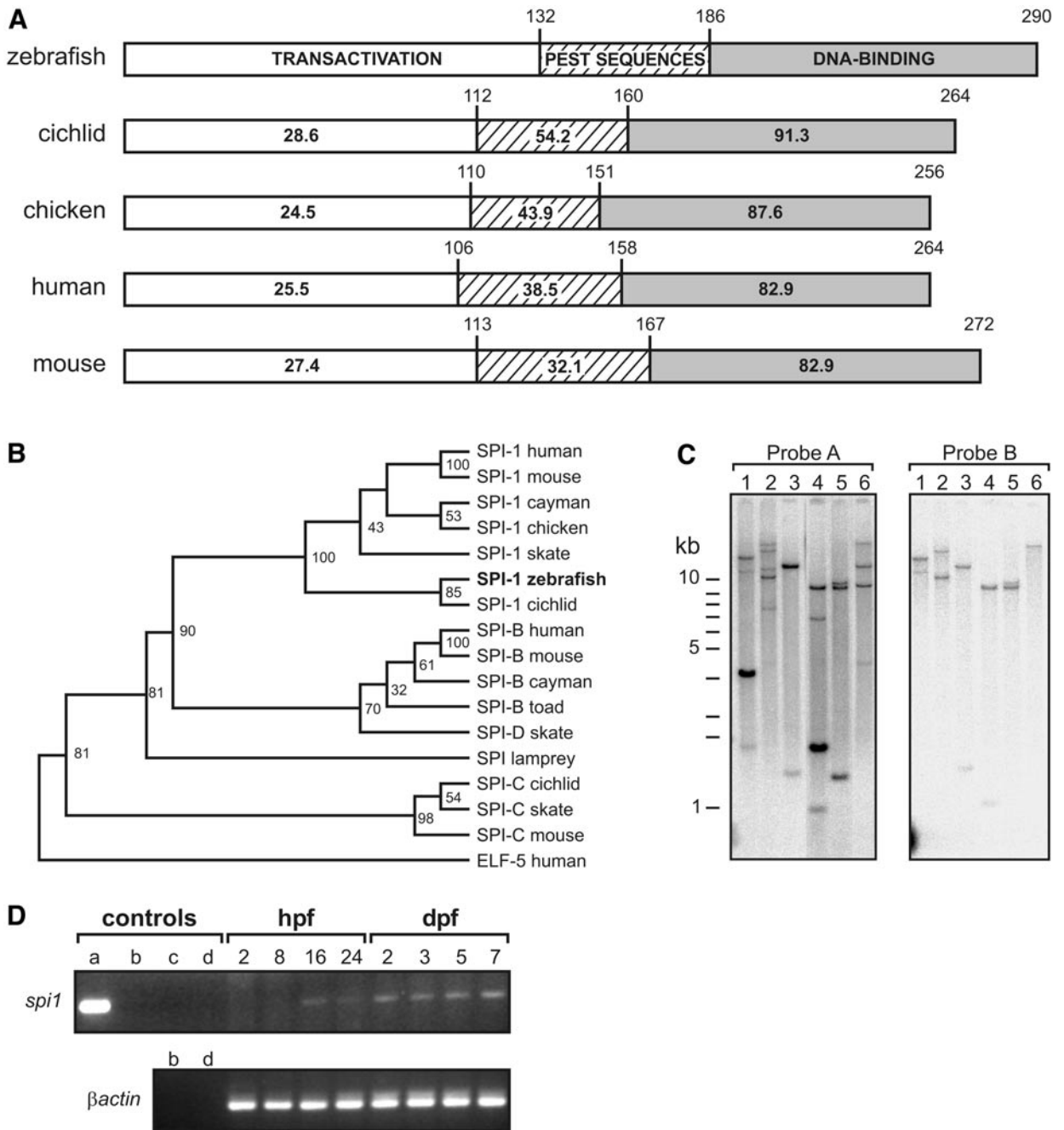
FIG. 1. A zebrafish *spi1* orthologue. (A) Comparison of functional domains of SPI.1 proteins from four species, showing amino acid identity scores for each of the three functional domains. In the box linear diagrams, numbers above domain boxes indicate the last residue of each functional domain, and numbers within indicate the percent identity to zebrafish *spi1*. (B) Phylogenetic analysis for amino acids demonstrates that *D. rerio spi1* is an orthologue of previously described SPI.1 genes, and that the related gene family members SPI-B and SPI-C form separate clades. [GenBank GI (or Accession) numbers, top to bottom: 4507175, 6755473, 8745406, 2369863, 11245497, (AF321099), 8745412, 36562, 2586116, 8745407, 8745409, 11245499, 8745404, 8745414, 11245501, 6755618, 4557551]. The analysis was based over the DNA binding domain for all proteins commencing at the sequence GX(R/K)(R/G/K)(K/R)XR in all but human ELF5, for which the sequence starting "TSLQSS" was used. The dendrogram was constructed by using ClustalX and Treeview building on the analysis of Spi family DNA-binding domains given in Shintani *et al.* (2000) and Anderson *et al.* (2001) using human ELF-5 as an outgroup. Bootstrap values (*n* = 1000) are indicated at nodes as percents. (C) Only one *spi1* gene exists in the zebrafish genome. Southern analysis of zebrafish genomic DNA digested with a various restriction enzymes (Lanes: 1, *Eco*RI; 2, *Bam*HI; 3, *Bgl*II; 4, *Pst*I; 5, *Xba*I; 6, *Sma*I) and hybridized to a radiolabeled probe corresponding to either the entire 1034 nucleotides (Probe A) or the first 367 nucleotides (Probe B) of the zebrafish *spi1* cDNA clone. A single band in lane 6 (probe B) indicates that this *spi1* gene fragment is represented in the zebrafish genome by one copy. (D) Survey of *spi1* expression in early zebrafish development by RT-PCR. Templates in control lanes (a–d) are: a, plasmid DNA; b, genomic DNA; c, water; d, RT-PCR without reverse transcriptase. Developmental ages from which RNA were prepared are 2, 8, 16, and 24 hpf and 2, 3, 5, and 7 dpf.
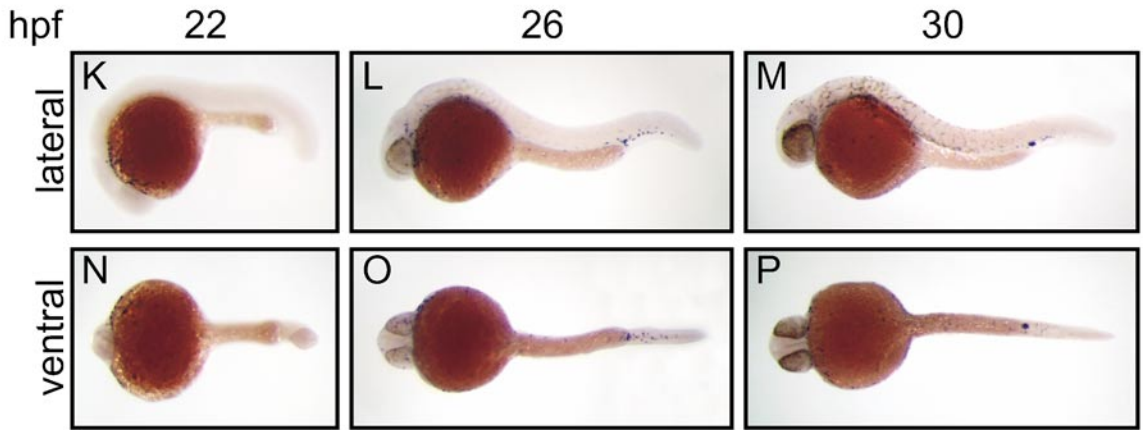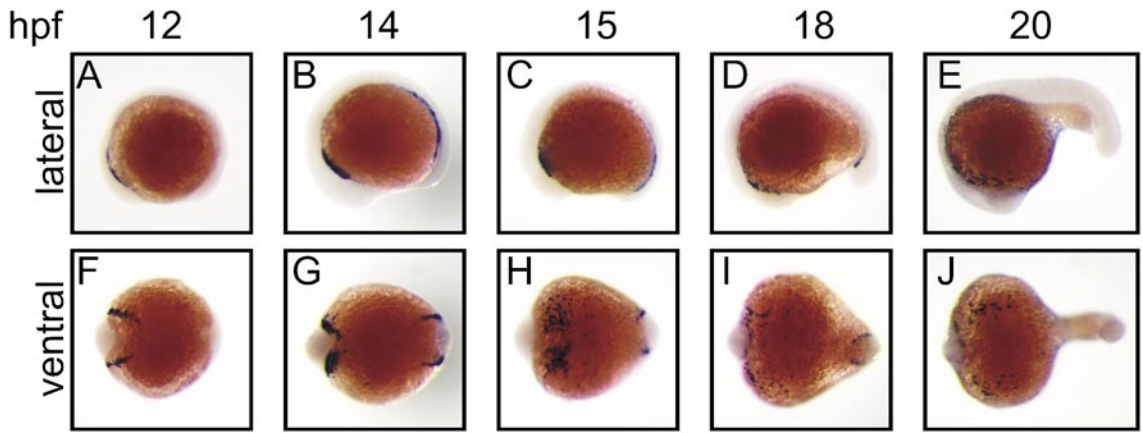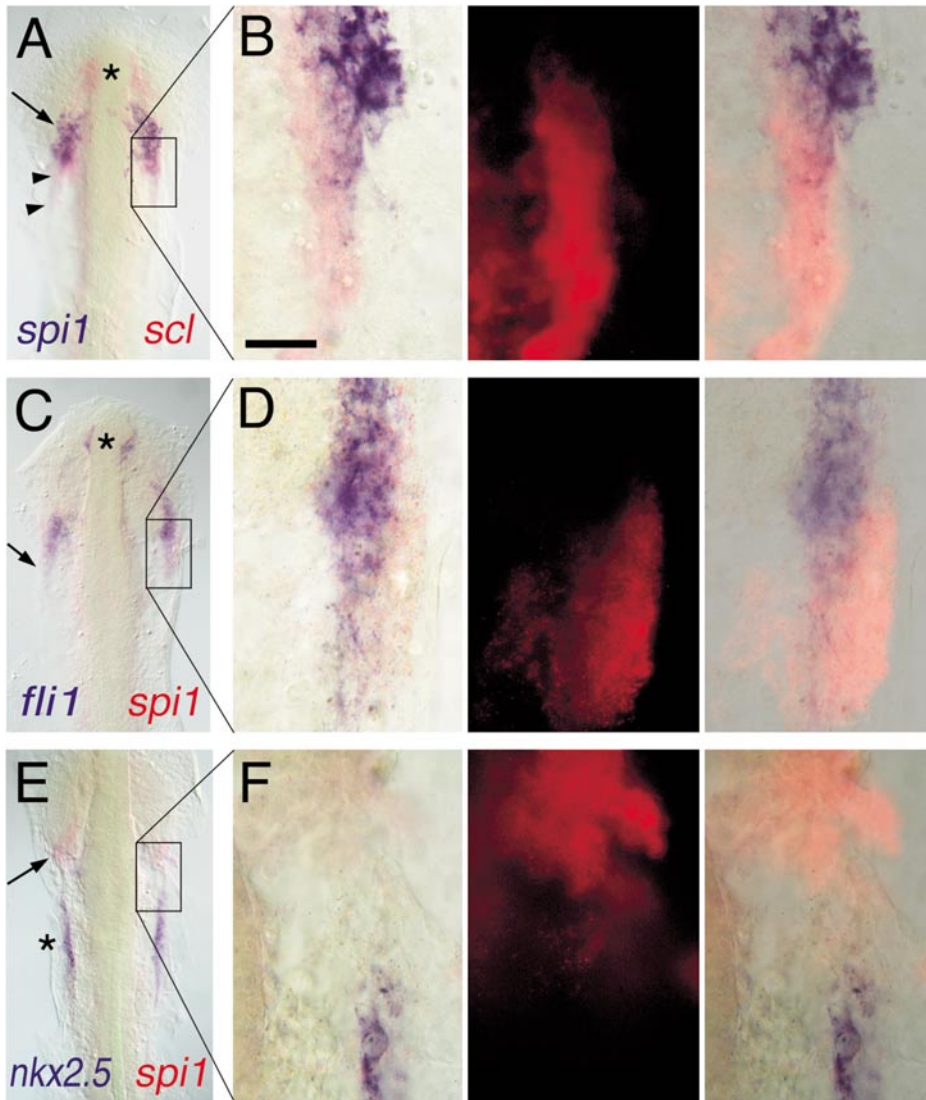
FIG. 4. Expression of *spi1* relative to other markers of lateral plate mesoderm fates. Two-color *in situ* hybridization gene expression analysis of wild-type zebrafish embryos (12 somite, flat mount, anterior up). Each panel in the left column shows a low-power view of the head and rostral lateral plate (A, C, E), and the corresponding three panels to the right show high-magnification views (63× water immersion lens) of particular regions of interest in which the expression of *scl* or *spi1* has been detected by fluorescence of Fast Red using an RITC filter set (B, D, F). In places, the presence of high levels of blue NBT/BCIP precipitate quenches the fluorescent signal. (A, B) *spi1* (blue) and *scl* (red). Asterisk marks rostral portion of *scl*$^+$/*spi1*$^-$ cells, arrow shows domain of *scl*$^+$/*spi1*$^+$ cells, and arrowheads show *scl*$^+$/*spi1*$^-$ cells caudal to the domain of coexpressing cells. (C, D) *fli1* (blue) and *spi1* (red). Asterisk marks rostral *fli1*$^+$/*spi1*$^-$ cells, and the arrow shows that, although *fli1* and *spi1* are largely coexpressed, at the lateral margin, some *fli1*$^-$/*spi1*$^+$ cells are evident. (E, F) *nkx2.5* (blue) and *spi1* (red). The heart anlage marked by *nkx2.5* (asterisk) is separate and caudal to the region of *spi1* expression (arrow). Scale bar in (B), 30 μm.

FIG. 2. Expression of zebrafish *spi1* in early embryonic development. Whole-mount *in situ* hybridization analysis of *spi1* expression in early zebrafish development. Panels show direct lateral (A–E, K–M) and ventral (F–J, N–P) views of embryos at each of the developmental times (hpf) indicated, with anterior to the left. In each case, the paired lateral and ventral views are of the same embryo. The results illustrated were generated with a 1034-nt riboprobe spanning the entire *spi1* cDNA; identical patterns were obtained with a 367-nt riboprobe corresponding to sequences encoding the more unique transactivation domain.

FIG. 3. Expression of *spi1* relative to *gata1* in the lateral plate mesoderm. Two-color *in situ* hybridization gene expression analysis of wild-type zebrafish embryo (12 somite, flat mount, rostral up). (A) A low-power view spanning the entire lateral plate mesoderm (LPM). (B, C) High-magnification views (63× water immersion lens) of regions boxed in (A), in which the expression of *spi1* has been detected by fluorescence of Fast Red using a RITC filter set. (B) *spi1*$^+$*gata1*$^-$ cells in the rostral LPM. Arrowheads indicate the caudal margin of the eye. (C) *spi1*$^+$*gata1*$^+$ cells in the caudal LPM. Arrowhead indicates an indentation to the otherwise uniform LPM *gata1*$^+$ domain, due to several cells that express neither *gata1* nor *spi1*. Arrow indicates a lateral irregularity in the LPM *gata1* domain, due to several cells that express both *gata1* and *spi1*. Scale bar in (B), 30 μm.

for imaging the red fluorescent dye. The paired images were then combined into a composite red on black and white image by using ImageJ 1.25s software (http://rsb.info.nih.gov/ij/).

RT-PCR Expression Analysis

Total RNA (1.5 μg) was reverse transcribed into cDNA by using 12.5 μM random hexamers, 8 mM MgCl$_2$, 1 mM of each dNTP, 1 U/μl RNase inhibitor, and 10 U/μl M-MuLV reverse transcriptase (New England Biolabs). Two microliters of the 20-μl reaction were used in a PCR containing 2.5 mM MgCl$_2$, 500 nM of each primer, and 0.2 U/μl *Taq* polymerase. PCR conditions were: 94°C 1 min, 52°C 1.5 min, 72°C 2 min, for 23 cycles, which preliminary experiments demonstrated to lie in the linear amplification range for these PCR products. Primer sequences were: *spi1*, 5′-CAGAATGGAGGGGTACAT-3′ and 5′-CGTTCTGACTGTCAT-CAA-3′; *βactin*, 5′-TGGCATCACACCTTCTAC-3′ and 5′-AGA-CCATCACCAGAGTCC-3′. PCR product sizes were: *spi1*, 200 nt; *βactin*, 221 nt.

Fate Mapping by UV Activation of Caged FITC-Dextran

Photoactivation of caged fluorescein was carried out as described (Kozlowski *et al.,* 1997). Briefly, early cleavage embryos were injected with 2% anionic DMNB-caged fluorescein-dextran (MW 10000; Molecular Probes, Eugene, OR) and stored in the dark until segmentation stages when they were transferred to a depression slide and oriented on 3% methyl cellulose with the lateral plate facing toward the objective. The slide was transferred to the stage of an Axioplan (Zeiss, Thornwood, NY) and the lateral plate was viewed with a 63× water immersion lens. The fluorescein was uncaged between 3 and 12 somites by a 5-s exposure of UV light (DAPI filter set) through a pinhole created by fully closing down the iris in the fluorescence light path. The site of photoactivation was immediately confirmed by using a low-light photomultiplier video camera (VS2000N-Rvideoscope International Ltd., Herndon, VA) and Cytos imaging software (ASI Inc, Eugene, OR) to prevent damage to the embryo from free radicals created by high-intensity fluorescence. Embryos were transferred to 24-well plates containing embryo medium and grown until the time of assay. The location of fluorescent cells was detected and scored initially by using a low-light photomultiplier video camera and Cytos imaging as above, and then embryos of interest were photographed by using Kodak Gold ASA100 print film on an Axiophot AX (Zeiss). Bright-field and fluorescent images were adjusted for contrast and merged by using Adobe Photoshop 5.5 software.

Injection of Zebrafish Embryos

Capped mRNA for microinjection was prepared by using mMessage mMachine kits (Ambion, Austin, Texas) using the following transcription templates, polymerase and linearizing enzyme combinations: for *Xenopus* chordin, pSP35T-chd (Sasai *et al.,* 1994), SP6, *Xba*I; for zebrafish *chordin*, pCS2+-chordin, SP6, *Not*I (Miller-Bertoglio *et al.,* 1997); for *Xenopus* BMP-4, BMP-4/pSP64T (Maeno *et al.,* 1996) SP6, *Bam*HI; and for enhanced green fluorescent protein (*EGFP*), pSP64TK-EGFP. The final resuspension of mRNA for injection was in water, the concentration determined spectrophotometrically, and mRNA integrity checked by visualization after denaturing formaldehyde agarose gel electrophoresis. One to four cell embryos were injected with approximately 600 pL containing 10–100 pg of mRNA by using a Leica stereomicroscope

(Wetzlar, Germany) and Narishige micromanipulators (Tokyo, Japan). Figure 7 data are representative of observations made from *Xenopus* chordin- or *BMP-4*-injected embryos, and control uninjected or diluent-injected embryos collected for analysis from several independent injection days. Observations of *spi1* and *gata1* expression were made in embryos selected from this collection, matched for both developmental age at the time of fixation, and morphologically for an equivalent degree of dorsalization or ventralization. Figure 8 data are representative of the spectrum of effects observed in *Xenopus* BMP-4- and zebrafish *chordin*-injected embryos collected from several independent injection experiments. In these experiments, *BMP-4* and *chordin* were coinjected with 10 pg of RNA-encoding EGFP, and only fluorescing embryos were included in the analysis. Control embryos were injected with 10 pg of *EGFP*-mRNA alone and showed a <5% abnormality rate (94 *EGFP*-injected embryos were distributed over the various subgroups to demonstrate the wild-type expression pattern in the *in situ* hybridization expression analysis). Noninjected embryos were also included as unmanipulated controls in each experiment.

Electron Microscopy

Embryos for electron microscopy were fixed in 2.5% glutaraldehyde and processed as described (Stanley *et al.,* 1994).

RESULTS

Zebrafish spi1 Transcript and Gene

A 1034-nucleotide cDNA encoding a zebrafish *spi1* orthologue was isolated by degenerate PCR and library screening (Genbank Accession No. AF321099). Conceptual translation revealed an open reading frame of 290 amino acids starting at nucleotide 15, although alternate candidate initiation ATG codons were located at downstream codons 22 and 54. *In vitro* translation of this cDNA recovered three polypeptides in approximately equal amounts, suggesting that all translational initiation start sites could be used *in vitro* at least (data not shown). The 290-amino-acid *spi1* protein showed 48.5–53.8% overall identity with mammalian, avian, and crocodilian PU.1, 57.2% identity with a cichlid PU.1, and only 28.2% identity with a lamprey SPI-1. Relative to mammalian and avian PU.1, homology was greatest in the DNA-binding domain, less in the central PEST sequences, and least in the N-terminal transactivation domain (amino acid identities of 83–91, 32–54, and 25–29%, respectively) (Fig. 1A). A phylogenetic analysis of SPI-family members (Fig. 1B) demonstrated that SPI-1 (PU.1) orthologues formed an independent clade to murine, human, toad, and crocodilian Spi-B orthologues (39.5–42.4% identity), and that murine and cichlid Spi-C formed a more distantly related clade again (25.2 and 21.9% identity, respectively).

Southern blot analysis of genomic zebrafish DNA digested with several enzymes using a full-length zebrafish *spi1* cDNA probe result resulted in multiple hybridizing bands, even at high stringencies. However, a shorter probe covering sequences confined to the transactivation domain (i.e., lacking sequences encoding the DNA-binding domain characterizing ETS family members, but still traversing 3

exons in the orthologous murine gene) (Moreau-Gachelin *et al.,* 1989) hybridized to a single band in a *Sma*I digest, confirming single copy representation of this gene in the zebrafish genome (Fig. 1C). The multiple hybridizing bands seen using the longer probe are likely due to separation of the multiple exons of the *spi1* genomic locus encompassed by the full-length cDNA probe onto several restriction digest DNA fragments, but may also reflect cross-hybridization to other ETS family members, in particular including other SPI-family members as have been described in other fish (Shintani *et al.,* 2000; Anderson *et al.,* 2001). We did not pursue further the possibility of other zebrafish *spi*-family members suggested by this analysis.

Zebrafish *spi1* was mapped to linkage group (LG) 7 on the LN54 radiation hybrid panel between markers Z21519 and Z9521 (at 111.3 and 116.12 cR), placing it near *groucho1* (at 111.4 cR). Mapping on the T51 panel placed it between z11894 and z21519 (at 1871.0 cR), also near *groucho1* (at 1865.0 cR). Human *PU.1* (*SPI1*) lies at 11p11.2, and murine *Pu.1* (*Sfpi1*) is located on chromosome 2 at 47.5 cM. Surveying the mapped genes in the vicinity indicates that zebrafish *spi1* lies in a LG7 region with a disjointed synteny to human chromosome 11 (Bertrand *et al.,* 2001; Yoder and Litman, 2000), and that this region shows less conserved genomic structure in mice. The syntenic relationships are not sufficiently conserved to contribute evidence to the orthologous relationship between *spi1* and *SPI1*.

Collectively, the structural, phylogenetic and genomic data indicate that the cDNA isolated is a zebrafish *spi1* orthologue.

Expression of spi1 during Early Zebrafish Development

RT-PCR was used to survey *spi1* gene expression during early development (Fig. 1D): *spi1* expression was absent prior to gastrulation (2 and 8 hpf), initiated during somitogenesis (16 hpf), and remained up to 7 days postfertilization (dpf). To identify the anatomic sites of early *spi1* expression in zebrafish embryos, whole-mount *in situ* hybridization analysis of zebrafish embryos was undertaken (Fig. 2).

spi1 expression first appeared in the rostral LPM at the 6-somite stage (12 hpf) (Figs. 2A and 2F). By 10-somites (14 hpf), rostral LPM expression had increased in intensity and extent, and single *spi1*-expressing cells began a process of dispersion, extending toward the midline underneath the developing animal axis, and laterally over the surface of the yolk (Figs. 2B and 2G). At this time, expression first appeared in the more caudal LPM (often referred to as "ventral" and/or "posterior") in a region identical with that previously described for *gata1* expression. Two-color *in situ* hybridization analysis confirmed that, in this caudal LPM domain, *spi1* and *gata1* expression overlapped on a cell-by-cell basis (Fig. 3), an exact concordance emphasized by several irregularities in the otherwise uniform stripe of LPM *gata1* expression (Fig. 3C). Rostrally, as expected, *spi1* expression was not accompanied by *gata1* (Fig. 3B).

Over subsequent hours, *spi1*-expressing cells dispersed

TABLE 1

Lateral Plate Mesoderm (LPM) Fate Varies According to Rostrocaudal Location

Region of LPM uncaged at the 3- to 12-somite stage	Score time (hpf)	Tissue marked	n_{marked}/n_{total}
Rostral, adjacent to eye[a]	24	Central nervous system	9/15
	24	Cranial mesenchyme[b]	5/15
	24	Vasculature	2/15
	24	Nonerythroid blood cells[c]	5/15
Somites 2–3	26	Posterior lateral line ganglia	8/12
	26	Primordial germ cells	10/12
Somites 6–8	26	Circulating erythrocytes	5/6
	26	Vasculature	2/6

[a] Illustrated in Figs. 5A and 5B.
[b] Illustrated in Fig. 5C.
[c] Illustrated in Fig. 5D.

over the surface of the spherical yolk sac from the rostral focus of LPM expression (Figs. 2C and 2H), so that by 18 hpf, the surface of the yolk was speckled with *spi1*-expressing cells, with their density usually greater over the rostral half of the yolk surface (Figs. 2D and 2I). The greatest extent of *spi1* expression occurred at 16–18 hpf, and following this, the number of *spi1*-positive cells and intensity of expression in all three regions waned (Figs. 2E and 2J). The domain of *spi1*-expression in the caudal LPM disappeared by 20 hpf (Figs. 2E and 2J). Embryos at 22–24 hpf generally retained only a few *spi1*-positive cells on the yolk surface (Figs. 2K and 2N). In a finely controlled time course experiment, caudal *spi1* expression was evident in 3/29 20-hpf embryos, but 0/46 22- to 24-hpf embryos. This reduction in *spi1* expression at 24 hpf was also evident in the semiquantitative RT-PCR analysis of gene expression (Fig. 1D). Over the period between 26 and 30 hpf, a small number of *spi1*-expressing cells were located in the posterior intermediate cell mass in the region where *gata2* expression had been previously described (also called the "posterior blood island"), and sometimes accompanied by scattered *spi1*-expressing cells in the axis of the embryo and over the yolk (Figs. 2L–2P). No further expression was seen by whole-mount *in situ* hybridization analysis of embryos up to 7 dpf, although by the more sensitive RT-PCR, transcripts could be demonstrated in embryos continuously up to this age (Fig. 1D). Identical patterns of expression were seen with riboprobes corresponding to either the first 367 nucleotides or entire 1034 nucleotides of the *spi1* cDNA, eliminating the possibility that the anatomically separate rostral and caudal sites of LPM expression might represent transcripts of different ETS-family members cross-hybridizing with the longer riboprobe.

We examined the rostral *spi1* expression domain relative to other markers of rostral LPM fates by two-color *in situ* hybridization at the 12-somite stage (Fig. 4). The transcrip-
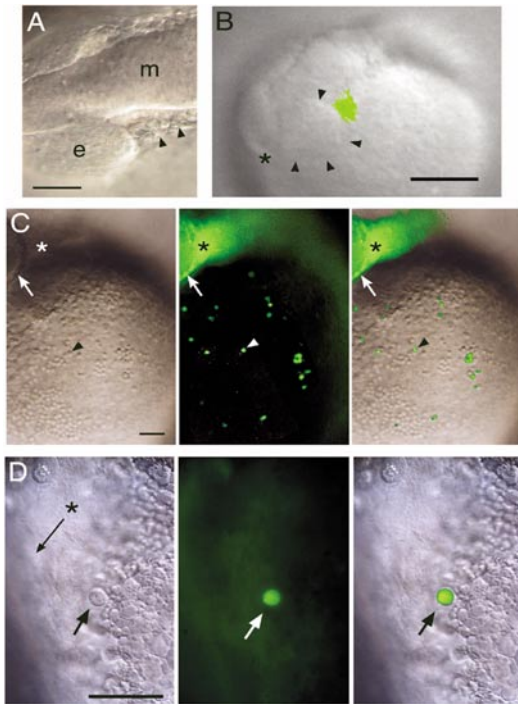
FIG. 5. Fate mapping of rostral lateral plate mesoderm cells. (Animals are positioned with rostral to the left and dorsal up.) (A) White light image of illustrating the cells targeted for uncaging at 12 somites (arrowheads). e, eye; m, midbrain. Scale bar, 50 μm. (B) Video capture of a freshly labeled embryo at 13 somites, with uncaged cells shown in green by overlay from a fluorescent image. Arrowheads mark the caudal rim of the eye, asterisk marks the rostral end of the central nervous system. Scale bar, 100 μm. (C) The same embryo after the onset of circulation. The arrow marks the caudal rim of the eye, the asterisk the site of uncaging in the side of the head, and the arrowhead one of the large round fluorescent cells (left panel, white light image; middle panel, fluorescent image; right panel, merged image). Scale bar, 100 μm. (D) At higher magnification, a large round cell (arrow) is shown in the Ducts of Cuvier. The asterisk and arrow indicate the main channel in which red blood cells flow, but they cannot be seen in this image because they are moving too fast (left panel, white light image; middle panel, fluorescent image; right panel, merged image). Scale bar, 50 μm.

tion factor *scl* is an early marker of hematovascular cell fate (Liao *et al.,* 1998): *spi1*-expressing cells are nested within a domain of *scl*-expressing cells (Figs. 4A and 4B). *fli1* is an early marker of vascular commitment (Thompson *et al.,* 1998): even though *fli1* and *spi1* are largely coexpressed, a group of *spi1*[+]/*fli1*^{−} cells is located at the lateral limits of the LPM (Figs. 4C and 4D). Hence, *spi1* expression defines a subset of *scl*-expressing cells, likely to be destined for hematopoiesis since some of them do not coexpress the vascular marker *fli1*. These *spi1*[+]/*scl*^{+} cells are rostral to and separate from the heart anlage marked by *nkx2.5* expression (Figs. 4E and 4F).

Rostral Zebrafish spi1 Expression Marks a Myeloid Cell Fate

spi1 expression directs a hematopoietic cell fate in other vertebrates, and in particular, specifies a myeloid rather than an erythroid fate (Rekhtman *et al.,* 1999), so we hypothesized that it would serve an analogous function in zebrafish. Since *spi1* is expressed first in the rostral LPM, we determined the developmental fate of rostral LPM cells by activation of caged fluorescein-dextran (Table 1 and Fig. 5), following the fate of caudal LPM cells as a control. Cells located in the caudal LPM early in somitogenesis frequently ended up as circulating erythrocytes, consistent with previous observations from *gata1* and *globin* gene expression (Detrich *et al.,* 1995; Chan *et al.,* 1997). In contrast, uncaged fluorescein-marked rostral LPM cells (Figs. 5A and 5B) contributed to a range of tissues (Fig. 5C), and in 33% (5/15) cases, could be identified as large round nonerythroid cells in the nascent circulation (Fig. 5D). These cells exhibited a range of behaviors consistent with a macrophage identity, including extension of pseudopodia, rapid changes in cell shape, and phagocytosis of debris and erythrocytes (not shown), indicating that they are similar or identical to the macrophages identified by videomicroscopy by Herbomel *et al.* (1999). Thus, cells in the *spi1* expression domain of the rostral LPM give rise to myeloid cells during embryogenesis.

spi1 Expression in Hematopoietic-Failure Mutants

The mutant *cloche* (*clo*) fails to initiate hematopoiesis and vasculogenesis due to a genetic lesion lying upstream of the early hematopoietic fate-specification transcription factor, *scl* (Liao *et al.,* 1998). Embryos homozygous for the severe *clo*[m39] allele show loss of early *scl* expression in both the rostral and caudal LPM, and erythropoietic failure at 24 hpf is reflected in the loss of *gata1* expression in caudal LPM during somitogenesis (Thompson *et al.,* 1998). We evaluated *spi1* expression in *clo*[m39] mutant embryos. There was total loss of rostral and caudal *spi1* expression (Figs. 6A and 6B), supporting the hypothesis that *spi1* marked cells with a hematopoietic fate.

The mutant *spadetail* (*spt*[b104]) has defective trunk mesodermal development consequent to a lesion in the *tbx16* gene (Ruvinsky *et al.,* 1998; Griffin *et al.,* 1998), which, despite expression of earlier hematopoietic lineage commitment markers such as *lmo2* and *gata2*, results in erythropoietic failure evidenced by reduced expression of *gata1* and *cmyb* in the ICM (Figs. 6C and 6D) (Thompson *et al.,* 1998). We used *spi1* expression to evaluate myeloid development in *spt* mutants. Although *spt* mutants showed loss of caudal LPM *spi1* expression, the rostral domain of *spi1* expression was preserved (Figs. 6E and 6F), consistent with normal rostral development in these mutants. Furthermore, electron microscopic examination of *spt* mutants at 48 hpf confirmed the presence of myeloid granulocytic cells (3/3 surveyed embryos), evidenced by their distinctive intracytoplasmic granules (Figs. 6G and 6H).
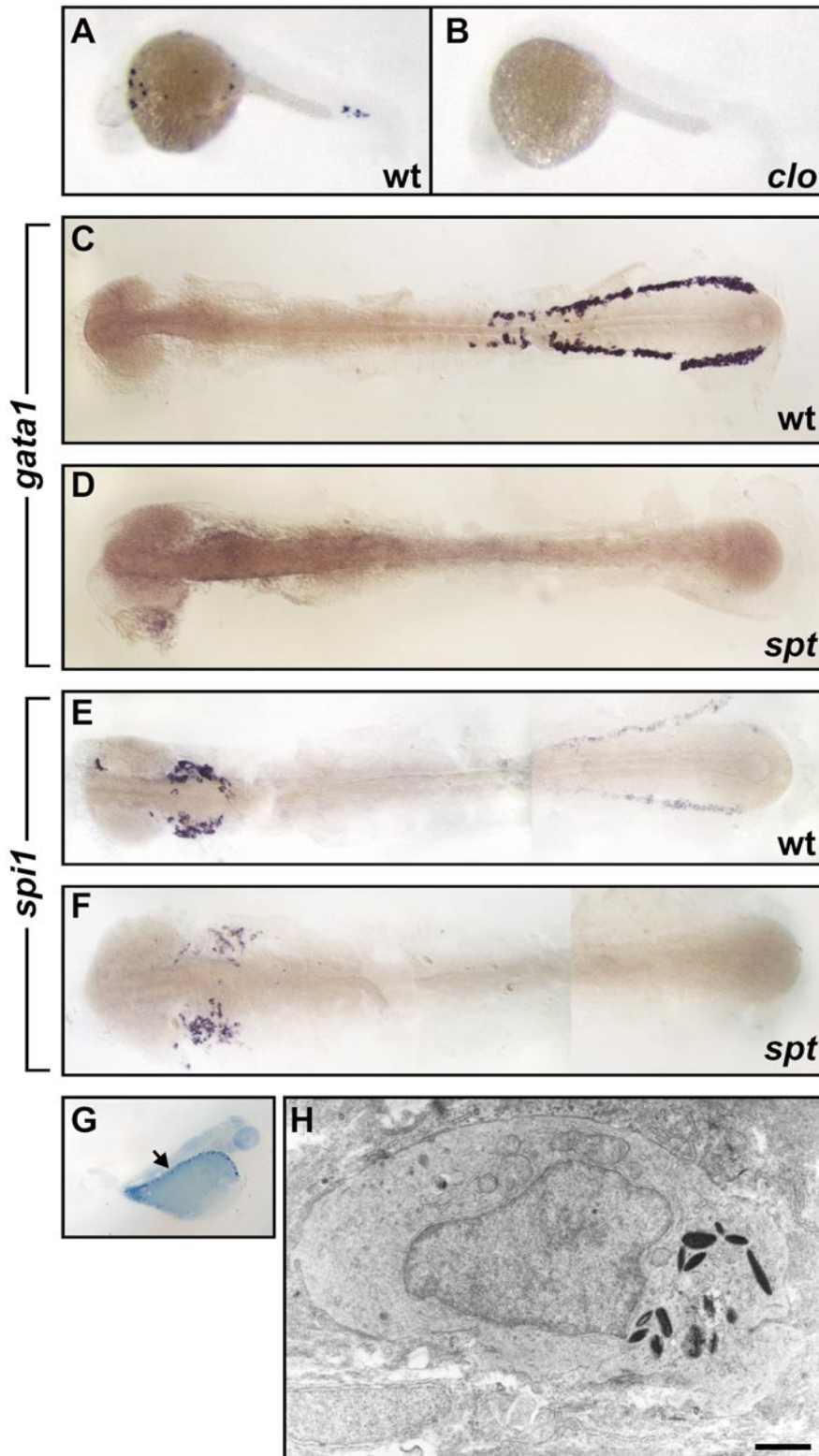
FIG. 6. *spi1* expression in the hematopoietic failure mutants *cloche* (*clo*) and *spadetail* (*spt*). (A, B) Whole-mount *in situ* hybridization demonstration of location of *spi1* expression in wild-type (A) and clo^{m39}/clo^{m39} (B) zebrafish (20 hpf), showing loss of expression in the *clo* mutant. At this age, *clo* homozygotes could not be recognized on the basis of coincident morphological features, but the expected

Rostral spi1 Expression and Myeloid Cell Fate Occur Independently of BMP Signals Required for Erythropoiesis

The initiation of myelopoiesis despite the failure of erythropoiesis observed in *spadetail* embryos led us to hypothesize that it may be possible for myelopoiesis to initiate, despite the absence of signals necessary for erythropoiesis. We tested this hypothesis by evaluating *spi1* and *gata1* expression in embryos with decreased or increased levels of BMP signaling by overexpression of both the BMP-antagonist *chordin* and *BMP-4*.

Embryos affected by *chordin* overexpression were readily identified after 16 hpf by their diminutive tail development, and such embryos retained a widely dispersed population of *spi1*-expressing cells over the rostral yolk, despite a marked reduction in the extent of *gata1* expression (Figs. 7A–7D). Embryos strongly affected by *BMP-4* overexpression retained a small number of dispersed *spi1*-expressing cells when assessed at 12–14 hpf (Figs. 7E–7H), although the rostrocaudal origin of these cells is unknown. At 24 hpf, rostral *spi1* expression was completely absent, despite obvious reduction in head development and enlarged tails of the embryos, with expansion of *gata1* expression in the posterior ICM (Figs. 7I–7L). Thus, the *spi1*-positive myeloid cells of the rostral domain behaved in these assays much as the notochord does, being reduced by an increase, and unaffected by a decrease in BMP signaling (Nikaido *et al.,* 1997).

We extended these observations by assessing the effect of *chordin* and *BMP-4* overexpression on other LPM fates along the rostrocaudal axis, using the rostral domain of *spi1* as a marker of rostral LPM fate; *nkx2.5* as a marker of the heart anlage, an intermediate LPM fate; *gata1* as a marker of caudal LPM fate, with *krox20* as an reference point for rostral–dorsal development and *myod* as an anchor for caudal–dorsal development. Embryos were graded morphologically into groups of those either severely, moderately, or mildly affected, collected at approximately 14–16 hpf or 24–26 hpf, and subjected to two-color *in situ* hybridization analysis for various combinations of these markers.

Moderately *BMP-4*-affected embryos scored at 14–16 hpf, with normal caudal morphology but diminutive head development, displayed loss or marked reduction in rostral domain of *spi1*, but showed a preserved (or possibly increased) posterior domain of *spi1* expression (Figs. 8A–8C), indicating that *spi1* expression in these two domains was independent of each other. In such embryos, the extent and pattern of *gata1* and *myod* expression was largely unaffected (Fig. 8H), and *nkx2.5* expression was reduced to a single spot of rostral expression (Fig. 8J), instead of the normal pattern of two lateral stripes (Figs. 8I and 8K, embryo "a"). More severely affected embryos, with grossly disturbed morphology, showed preservation or even expansion of a distorted posterior domain of *spi1* expression (Fig. 8D), which was analogous to the expanded distorted domains of *gata1* expression observed in such embryos (Fig. 8E), although it proved technically very difficult to demonstrate this together in the same embryos, due to quenching of the red *gata1* signal by the extensive blue *spi1* signal. In such severely affected embryos, *nkx2.5* expression was sometimes absent, despite expanded *gata1* expression in the same embryo (Fig. 8K). Hence, the most rostral fate (marked by rostral *spi1*) was more sensitive to abrogation by excess BMP-4 signaling than the intermediate fate (marked by *nkx2.5*), and neither was expanded in circumstances when caudal fates were (caudal *spi1* and *gata1*, and *myod*; data not shown).

Moderately *chordin*-affected embryos scored at 14–16 hpf, with normal rostral morphology but diminutive tail development, displayed preservation of the full extent of rostral *spi1* expression (Fig. 8L), despite marked reduction in the extent of caudal *spi1* expression (Fig. 8L) and *gata1* expression (Fig. 8N). The normal rostral–dorsal development of such embryos was confirmed by preservation of the typical pattern of *krox20* expression (Fig. 8M). Even in embryos with diminutive *gata1* expression, *nkx2.5* expression remained bilateral and approximately normal in degree, although in some embryos, its rostrocaudal dimension was shortened (Fig. 8N). Of 24 embryos affected to varying degrees, 23/24 were *gata1*+/*nkx*+ and 0/24 lacked expression of one or other marker (1 was unscorable), suggesting that *chordin* antagonism of BMP signaling could not completely abrogate *gata1* expression, even in the most severely affected embryos. Similar observations were made in embryos scored at 24–26 hpf: extensive rostral *spi1* expression was retained in embryos with a mere nubbin of a tail (Figs. 7D and 8O), with retention of *nkx2.5* expression to a far greater degree than for *gata1*, which was reduced to a small region underlying the small stubby tail (Fig. 8P). Hence, the most rostral LPM fates can proceed independently of caudal BMP signaling, and the more rostral the fate, the less it is affected by *chordin* overexpression.

Collectively, these gain-of-function experiments indicate that rostral myeloid specification can occur despite marked

---

proportion (29/109, 27%) of embryos from the mating of *clo* heterozygotes showed the appearance in (B). (C–F) Flat preparations of whole-mount *in situ* hybridization preparations of 14-somite wild-type (C, E) and *spt*[b104]/*spt*[b104] (D, F) zebrafish embryos. Expression of *gata1* in the caudal LPM is present in the wild-type (C) but not *spt* (D) embryo. (E, F) Rostral *spi1* expression is retained in the *spt* embryo, despite loss of caudal LPM *spi1*-expressing cells. Panel (F) is representative of *spi1* staining in 14 *spt* embryos in a clutch of 54 (26%) resulting from *spt*[b104/+] interbreeding. (G, H) Myelopoiesis initiates in *spt* mutants despite erythropoietic failure. Methylene-blue-stained thick section of a 48-hpf *spt* embryo (G), indicating (arrow) the location of the granulocyte identified on electron microscopy by its characteristic cytoplasmic electron-dense elliptical granules (H).

diminution or even abrogation of the BMP signals required for erythroid specification, and vice versa, that caudal erythroid specification is not dependent on the signal(s) required for *spi1*-marked myeloid specification. To confirm and extend these observations, we next examined the development of myeloid and erythroid cells in zebrafish carrying loss-of-function mutations in *chordin* and *bmp* genes.

Loss of *chordin* function during early embryogenesis gives rise to the *chordino* (*dino*) mutant phenotype, which shows a reduction in rostral notochord and head structures and a dramatic increase in the production of erythroid cells (Hammerschmidt *et al.,* 1996a,b; Mullins *et al.,* 1996). This phenotype is thus overtly similar to, but slightly weaker than, that seen after BMP-4 overexpression. Examination of *spi1* expression in *dino* mutants showed a rostral domain that is compressed along the rostrocaudal axis and broadened mediolaterally, and a normal caudal domain (Figs. 9A and 9B). The expression of early hematopoietic and vascular markers *scl* and *fli1* was similarly compressed rostrally, and was greatly expanded in the caudal embryo (Figs. 9C–9F), consistent with the previously demonstrated increase in erythroid cells (Hammerschmidt *et al.,* 1996a,b; Mullins *et al.,* 1996). These data indicate that *spi1*-positive myeloid cells do not require *chordin* for their development, and are specified under conditions that cause the absence or reduction of the anterior notochord.

Loss of zebrafish *bmp2b* function results in the *swirl* (*swr*) mutant phenotype, which shows a diminutive tail and lacks erythroid cells and other caudal–ventral structures, but retains a notochord (Mullins *et al.,* 1996; Kishimoto *et al.,* 1997). The *swr*[ta72] allele results from a 6-amino-acid C-terminal extension of the mature protein that gives a dominant negative effect, resulting in a mild heterozygous dominant phenotype. Loss of *bmp7* function results in the *snailhouse* (*snh*) mutant, the *snh*[ty68] allele of which is due to a point mutation in the *bmp7* prodomain. This phenotype resembles a partially *bmp2b*-rescued *swr* mutant (Dick *et al.,* 2000), and has reduced or absent *gata1* expression (Mullins *et al.,* 1996), depending on the phenotypic strength which varies between mating pairs. Thus, these phenotypes show similarity to that seen after *chordin* overexpression, and comprise a phenotypic series of embryonic defects due to increasingly reduced BMP signaling. In both of these mutants, *spi1* expression is present but its onset is temporally delayed (Figs. 10A–10C). At later stages, increasingly severe *snh* and *swr* mutant phenotypes show first a loss of the caudal domain of *spi1* expression and then progressive diminution in the extent of rostral *spi1* expression (Figs. 10D–10I). In stage- and phenotype-matched *swr*[ta72] embryos from the same clutches, *gata1* expression paralleled that of the *spi1* caudal domain and was severely reduced or absent (data not shown). Thus, a reduction of BMP signaling to levels that abolish erythroid development does not significantly affect rostral *spi1* expression, consistent with the overexpression experiments presented above.

DISCUSSION

We have cloned a homologue of mammalian *SPI-1* (*PU.1*) that meets several criteria for identification as the zebrafish orthologue: there was high sequence conservation in the DNA binding domain; zebrafish *spi1* segregated with other *SPI-1* orthologues and not with other *SPI* family members in a cladistic analysis of this domain; and *spi1* and *SPI1* are positioned on zebrafish LG7 and human chromosome 11, respectively, in the context of a conserved but disjointed syntenic relationship between these chromosomes. Fate-mapping of rostral LPM cells from the region of *spi1* expression to large nonerythroid cells in the nascent circulation confirms *spi1* as an early marker of myeloid differentiation, suggesting that its biological role in mammals and zebrafish has been conserved.

spi1 Marks a Rostral Site of Early Myeloid Development in Zebrafish Embryos

The expression pattern of *spi1* indicates that myeloid differentiation starts at a rostral site, anatomically separate from early *gata1*-marked erythroid development. Previous videomicroscopic studies in zebrafish identified mobile phagocytes emanating from a site just anterior to the developing heart, and described two markers of this population of phagocytic cells: *draculin* and *l-plastin* (Herbomel *et al.,* 1999). Although *draculin* is expressed in the myeloid cells dispersing from the rostral LPM over the yolk sac during segmentation, it is also expressed throughout the lateral plate primordium from midgastrulation and persists in both differentiated macrophages and erythrocytes, suggesting a nonlineage-restricted general role in hematopoietic commitment, rather than one focused on myeloid fate per se. *l-plastin*, a marker of maturing macrophages, is expressed only as these cells migrate onto the yolk sac (Herbomel *et al.,* 1999). In contrast, we have isolated a gene (*spi1*) which preferentially marks myeloid fate, and this has enabled us to distinguish between cells committing to myelopoiesis and those committing to another hematopoietic fate. At the onset of *spi1* expression at 12 hpf (6 somite), expression is confined to a tight group of cells in a specific region of the rostral LPM that we have demonstrated is fated to a myeloid outcome. This makes it the earliest myeloid-specific marker identified in zebrafish to date. Later, *spi1* expression is observed in the caudal LPM. We have not determined the functional role of *spi1* expression in the caudal LPM. Given the interaction between Spi-1 and Gata-1 in mammalian systems (Rekhtman *et al.,* 1999; Zhang *et al.,* 2000), *spi1* may serve to regulate or even limit the degree of erythroid commitment in this region of the zebrafish embryo by an interaction with *gata1*. Another possibility, given that neonatal phenotypes of Spi-1-deficient mice implicate mammalian Spi-1 in the development of granulocytic, macrophage, and lymphoid lineages (Scott *et al.,* 1994; McKercher *et al.,* 1996), is that the different domains of its expression may reflect roles specific to the various myeloid lineages, and that the ICM may give
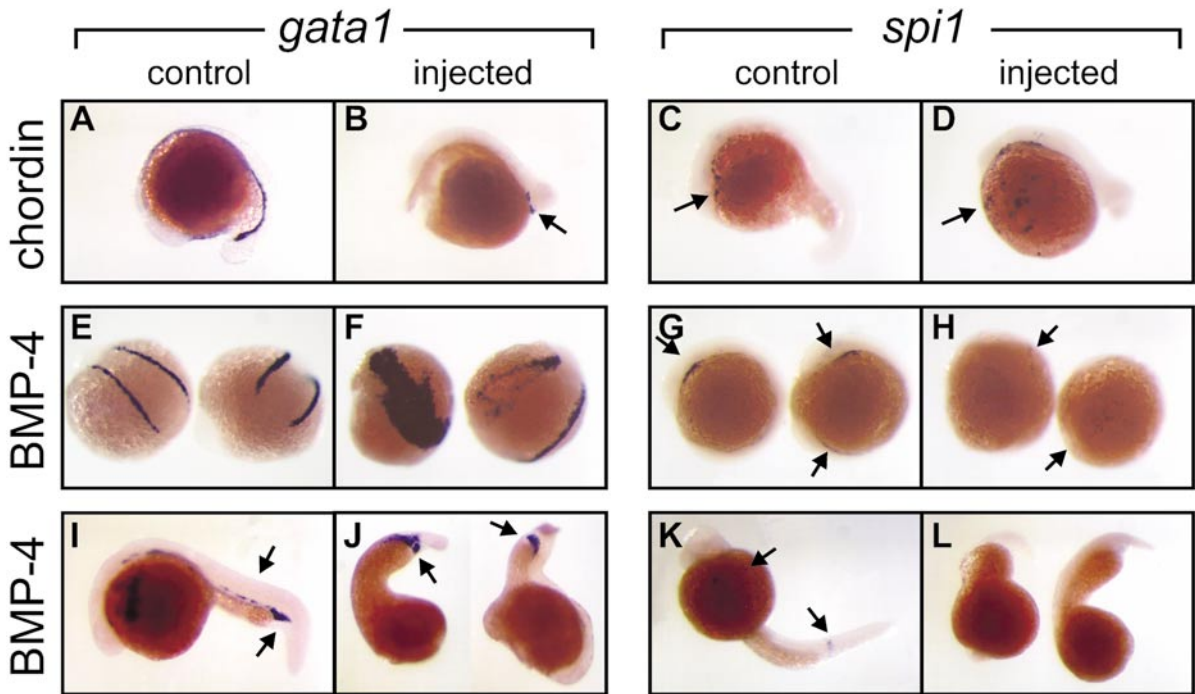
FIG. 7. Caudal erythroid commitment (marked by *gata1* expression) and rostral myeloid commitment (marked by *spi1* expression) can proceed independently of each other. Whole-mount *in situ* hybridization preparations displaying regions of *gata1* and *spi1* expression in embryos either untreated (control) or injected with mRNA encoding the *Xenopus* BMP-4 or chordin proteins as indicated to the left. (A–D) Nontreated (A, C) and *chordin* mRNA-injected (B, D) embryos at 18–20 hpf showing that *chordin*-expressing embryos have reduced *gata1* expression (arrow A, B) in the caudal intermediate cell mass (ICM) but retain rostral *spi1* expression in the lateral plate mesoderm (LPM) (arrow, C, D). (E–H) Nontreated (E, G) and *BMP-4* mRNA-injected (F, H) embryos at 12–14 hpf showing that *BMP-4*-expressing embryos have reduced extent of *spi1* expression (arrow, G, H) but a markedly expanded domain of *gata1* expression (arrow E, F). (I–L) Nontreated (I, K) and *BMP-4* mRNA-injected (J, L) embryos at 24 hpf showing *BMP-4*-expressing embryos have reduced extent of *spi1* expression (arrow, K) but a markedly expanded domain of *gata1* expression in the posterior ICM (arrow, I, J). Images are illustrative of 169 *Xenopus* chordin-injected (53% severe, 47% moderate-mild) and 204 *BMP-4*-injected (44% severe, 56% moderate-mild) and control uninjected or diluent-injected embryos, collected for analysis from several independent injection days (*BMP-4*, $n = 11$; *chordin*, $n = 6$).

rise to a small number of previously undetected myeloid cells in addition to a multitude of erythrocytes.

Rostral Myeloid Development Is Not Dependent on Erythroid Fate-Determining Signals

Evidence for the spatial separation of cells committed to different rostrocaudal LPM fates before gastrulation. Specification of distinct hematopoietic fates could be established as early as pregastrula stages, or it might be the result of interactions at a later stage between a developmentally naïve lateral plate and inducing substances with restricted rostrocaudal distribution in a neighboring tissue, such as the somites. The fate-mapping studies of Herbomel *et al.* (1999) based on cleavage (16-cell stage) cell labeling suggest that myeloid and erythroid lineages both appear to be derived from the part of the pregastrula embryo opposite the shield, at the ventral end of the proposed early dorsoventral axis.

Our observations support the notion of distinct genetic control for the specification of the myeloid and erythroid lineages in the pregastrulation zebrafish embryo. Overexpression of BMPs has previously been interpreted to result in the respecification of the cells of the early zebrafish gastrula to a more ventral fate, whereby the most dorsal fates, such as notochord, are lost, and the number of cells expressing ventral fates, such as erythrocytes, is dramatically increased in the resulting embryo (Neave *et al.,* 1997; Nikaido *et al.,* 1997). In embryos strongly affected by *BMP-4* overexpression, we observe that, despite a dramatic increase in erythrocytic fate, there is a near total loss of myeloid cells, suggesting that specification of myeloid cells cannot occur under the same high levels of BMP signaling that favor erythroid production. Conversely, in embryos overexpressing the BMP antagonist *chordin*, and in embryos with reduced BMP signaling due to loss-of-function mutations in *bmp2b* and *bmp7*, the production of myeloid cells is not affected, despite the near total loss of the
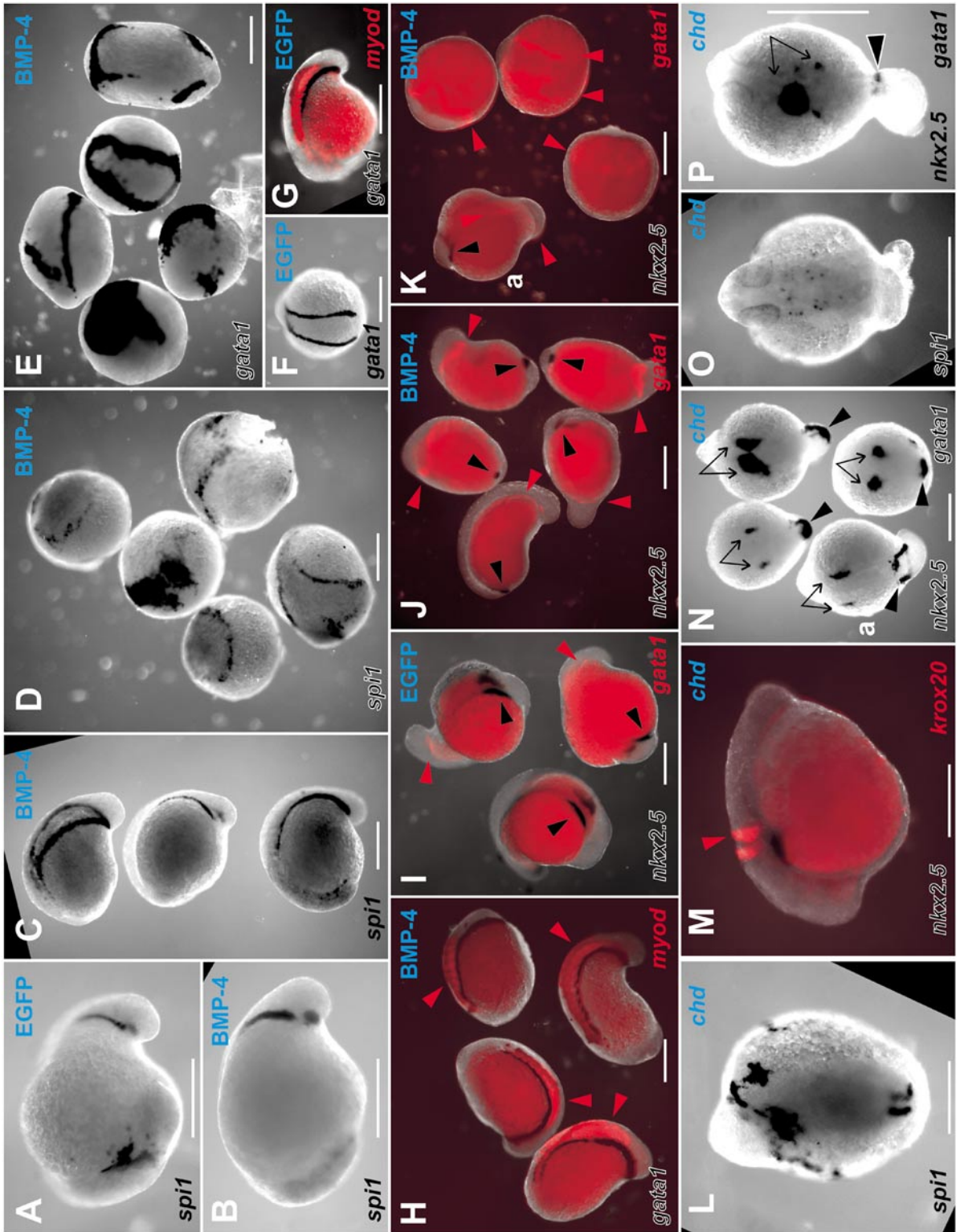
erythroid lineage, suggesting that that myeloid cells can be specified and develop normally without the high levels of BMP signaling typical of the region of the early gastrula opposite the shield. Thus, in these assays, myeloid cell specification does not exhibit the characteristics expected of a tissue derived from the same region of the gastrula as erythroid cells, seemingly at odds with the allocation of the pregastrula origins of this lineage as obtained by cleavage stage cell labeling to a position at the ventral end of the proposed early dorsoventral axis (Herbomel *et al.,* 1999). We note that a clone of cells descended from a blastomere labeled at the 16-cell stage will undergo considerable dispersion through radial intercalation before the onset of gastrulation (Wilson *et al.,* 1995), potentially spreading to regions of the pregastrula where cells experience lower levels of BMP signaling than at the ventral end of the proposed dorsoventral axis.

Indeed, careful examination of the results of the fate-mapping experiments (Herbomel *et al.,* 1999) indicate that it is possible to mark one lineage of embryonic blood cells without the other, suggesting that even at this early stage, their precursors may be spatially distinct. In cases where only one lineage was labeled, cells of the heart were sometimes colabeled, and this occurred more frequently for myeloid (2/3) than erythroid (1/7) cells, suggesting that myeloid precursors in the pregastrula are closer to the precursors of the heart than are erythroid precursors. This hypothesis is consistent with our results in segmentation stage embryos showing myeloid cells positioned in the anterior LPM rostral and immediately adjacent to the heart field, whereas the most rostral erythroid cells are found ventral to somite 6 in the trunk.

In further support of this hypothesis, fate mapping by following single cells at gastrula stages has demonstrated the origin of the head vasculature in a location adjacent to the notochord anlage (Warga and Nusslein-Volhard, 1999). This observation combined with our data showing that *spi1*-expressing myeloid precursors overlap with the *fli1*-positive cells of the nascent head vasculature in the rostral LPM also implies a common pregastrulation origin for both head vasculature and myeloid cells near the dorsal end of the proposed early dorsoventral axis. Combined, these data argue for a genetically distinct specification of spatially separated hematopoietic lineages before the onset of gastrulation. Thus, our observations do not support a model in which the default differentiation pathway of hematopoietically fated ventral tissues is erythroid, and other hematopoietic fates are produced by lineage respecification away from an erythroid developmental pathway, for example, by *spi1* competing out a *gata1* effect at the stem cell level.

Our findings do not rule out the activity of additional permissive factors in the environment of the developing LPM that may be required for the progression or survival of the myeloid lineage in the postgastrulation embryo. It will be interesting to determine whether there are instructive signals that vary along the rostrocaudal axis of the LPM of postgastrula embryos that are responsible for the precise localization of its different fates; for example, there may be some role for the CNS or lateral epidermis in positioning the boundary between myeloid and heart fate. Such tissue

FIG. 8. Actions of BMP and chordin on the LPM to perturb the balance of rostrocaudal LPM fates. Whole-mount *in situ* hybridization preparations of zebrafish embryos displaying expression domains of various markers (indicated in lower lefthand corner of each panel), in *EGFP* mRNA-injected (A, F, G, I), *Xenopus* BMP-4 mRNA-injected (B–E, H, J, K) and zebrafish *chordin* mRNA-injected (L–P) embryos (injected mRNA indicated in top righthand corner of each panel). Embryos are variously orientated to optimally display the range of expression patterns of interest. (A–N) Embryos are at approximately 14 hpf; (O, P) Approximately 24 hpf stages of development. (A–D) *spi1* expression in control *EGFP*-injected (A), moderately (B and C), and severely (D) affected *BMP-4*-injected embryos. (A–C, approximately lateral views with head to the left; the five dysmorphic embryos in D are in various orientations.) (E, F) *gata1* expression in five severely affected *BMP-4*-injected embryos (E, various orientations), showing ectopic expression and expansion of *gata1* expression compared with the wild-type expression pattern observed in *EGFP*-injected embryos (F). (G, H) Group of four moderately *BMP-4*-affected embryos (H) displaying normal expression of *gata1* and *myod* (red arrowheads) (various orientations), compared with the wild-type expression pattern observed in *EGFP*-injected embryos (G). (I, J) Group of five moderately *BMP-4*-affected embryos (J) showing normal *gata1* expression (red arrowheads) but markedly diminished *nkx2.5* expression (black arrowheads) (various orientations), compared with the wild-type expression pattern observed in *EGFP*-injected embryos (I). (K) Three severely affected *BMP-4*-injected embryos showing expanded *gata1* expression and loss of *nkx2.5* expression, including a relatively unaffected embryo (upper left, marked "a") for comparison with rostral *nkx2.5* strips (black arrowhead) and caudal *gata1* stripes (red arrowheads). (L) Dorsal view (head at top) of a *chordin*-injected embryo showing extensive rostral *spi1* and diminished caudal *spi1* expression domains. (M) Lateral view (head to left) showing relationship of *nkx2.5* and *krox20* in moderately *chordin*-affected embryo. (N) Dorsal views (head to top) of three moderately *chordin*-affected embryos showing markedly reduced extent of caudal *gata1* expression (black arrowheads) and less affected more rostral *nkx2.5* expression (black arrows), with a minimally affected embryo (lower left, marked "a") for comparison. The wild-type expression pattern of these genes in EGFP-injected embryos is shown in two colors (G, I). (O, P) Dorsal views (head to top) of moderately affected *chordin*-injected embryos showing preserved dispersed *spi1* expression (O), bilateral *nkx2.5* expression (P, arrows), and small spot of *gata1* expression in tail stub (P, arrowhead). Images are representative of the spectrum of effects observed in 137 *BMP-4*- and 78 zebrafish *chordin*-injected embryos scored at ≈14 hpf (19/137 and 41/78 severely affected, respectively), and 154 *BMP-4*- and 66 *chordin*-injected embryos scored at ≈24 hpf (21/154 and 13/66 severely affected, respectively), collected from several independent injection days (*BMP-4, n = 3; chordin, n = 2*) and divided between the various groups of *in situ* hybridization analyses. In these experiments, control embryos were injected with 10 pg of mRNA encoding EGFP with a <5% abnormality rate (94 embryos, which were divided into groups to demonstrate the wild-type pattern for the various *in situ* hybridization expression analyses). Scale bars, 0.3 mm.

interactions are important in the separation of heart and erythroid fates (Marvin *et al.,* 2001; Tzahor and Lassar, 2001; Schneider and Mercola, 2001).

BMP signaling influences on rostrocaudal LPM fates. One interpretation of our observations is to think of the effects of BMP signaling, at least in so far as they affect a ventral, mesodermal structure like the LPM, as having differential effects along a rostrocaudal (i.e., anteroposterior) axis. Our observations of the effects of *BMP-4* and *chordin* overexpression on the rostral *spi1, nkx2.5,* and caudal *gata1, spi1* expression domains are consistent with this. *BMP-4* overexpression first suppresses the most rostral fate (rostral *spi1*), diminishes, and then in stronger phenotypes abolishes an intermediate LPM fate (the heart, marked by *nkx2.5*). In weak phenotypes, BMP-4 has little effect on caudal *gata1/spi1* expression domains, but at high doses, expands both. In contrast, the most caudal LPM domains (marked by *gata1/spi1*) are the most sensitive to overexpression of the BMP antagonist *chordin*, or to loss of endogenous *bmp* gene function. The intermediate LPM domain of the heart anlage marked by *nkx2.5* is less sensitive to the abrogation of BMP signals by *chordin* overexpression, or *swr* or *snh* genetic background, and the most rostral LPM domain (rostral *spi1*) is highly resistant to any reduction of BMP signaling, even in the most severely affected embryos.

Thus, it is tempting to suggest that BMP signaling in the early zebrafish embryo establishes the anterior–posterior axis of the mesoderm, not the dorsal–ventral axis. Consistent with this, in supposedly "ventralized" *BMP-4*-overexpressing embryos, the caudal-*dorsal* marker *myod* was retained, suggesting that the embryo was posteriorized. Conversely, in supposedly "dorsalized" *chordin*-overexpressing embryos, somite formation and *myod* expression were reduced (data not shown), suggesting that these embryos are anteriorized. The connection between anterior and dorsal in the zebrafish fate map has been previously appreciated (Kimmel *et al.,* 1990), and an explicit separation of dorsoventral and anterior–posterior axes has recently been achieved for the *Xenopus* gastrula that is in agreement with our findings (Lane and Smith, 1999; Lane and Sheets, 2000), suggesting that the assignment of the early axes may need to be reexamined. Our characterization of zebrafish *spi1* identifies for the first time in zebrafish a reagent that can distinguish rostral–ventral fates, and will be useful in the fine fate-mapping studies necessary to test this hypothesis.

The necessity of BMP and chordin signals for LPM fates, assessed by analysis of mutants. Interestingly, loss of the BMP-antagonizing function of *chordin* in *chordino* mutant embryos did not greatly affect *spi1* expression or other LPM fates, indicating that *chordin* is not required directly for myeloid specification. This observation indicates that any role for *chordin* in myelopoiesis may be restricted to that of a general BMP antagonist in the pregastrula. Moreover, the *chordino* mutant is not as severely affected as a strong *BMP-4* overexpression phenotype, perhaps because addi-

tional BMP antagonists, *noggin* and *ogon*, are likely active in this mutant embryo (Miller-Bertoglio *et al.,* 1999) and may function in the absence of *chordino* to reduce BMP signaling to levels compatible with myeloid development. The loss of caudal *gata1/spi1* expression in the weaker phenotypes of the *bmp* mutants *swr* and *snh* before any effect on rostral *spi1* is observed indicates the greater dependence of these caudal fates on the presence of BMP signals, but the delay and near abrogation of rostral *spi1* expression in more severe phenotypes underscores the dependence of these LPM fates on the presence of at least some BMP signals.

Conservation of a Rostral Origin for Embryonic Myeloid Cells in Vertebrate Evolution

The question arises as to whether the anatomical separation of the first sites of erythroid and myeloid commitment is peculiar to zebrafish, or if it represents a general aspect of vertebrate development. In *Xenopus*, studies using a leukocyte-marking monoclonal antibody and head–body chimeras have demonstrated that a macrophage population exists that does not arise from the ventral blood island nor the dorsolateral plate, but from a region of the rostral embryo anterior to the cardiac territory (Ohinata *et al.,* 1990; Miyanaga *et al.,* 1998). Also of interest is the observation that the early expression pattern of *Xaml1* (a *Xenopus* CBFA2/AML1 homologue) includes lateral plate mesoderm cells anterior to those of the ventral blood island that will later form erythroid cells (Tracey *et al.,* 1998).

In mice, several markers have been used to examine the first site of macrophage appearance and suggest that an early precirculation rostral site of macrophage production may occur in mice as well. The earliest cells stained with the antibody F4/80 (which identifies a macrophage antigen prevalent in all known murine macrophage populations) appeared in the visceral yolk sac blood islands, but it is also mentioned that in one 9-day conceptus, scattered F4/80-positive cells were also seen in the regions of the head, heart, and dorsal aorta (Morris *et al.,* 1991). *MITF* gene expression, also an early marker of macrophage development in the mouse, is described as appearing in the yolk sac, head, and a band above the developing heart simultaneously (Lichanska *et al.,* 1999). Expression of c-*fms*, the receptor for colony-stimulating factor-1 (the macrophage-specific hematopoietic growth factor) appears first in the yolk sac at 9.5 days. Lichanska *et al.* (1999) observe that the appearance of c-*fms*-expressing cells in the head of the embryo is never delayed relative to their appearance in the yolk sac, and comment that occasional embryos showed clustering in a band overlying the developing heart. A zebrafish orthologue of c-*fms* has been cloned, and the expression pattern is reported to follow that of macrophage precursors (Parichy *et al.,* 2000).

Spi-1 expression has also been examined in the developing mouse, but was not detectable by *in situ* hybridization before the onset of liver hematopoiesis (Lichanska *et al.,* 1999), and in particular, followed the appearance of c-*fms*
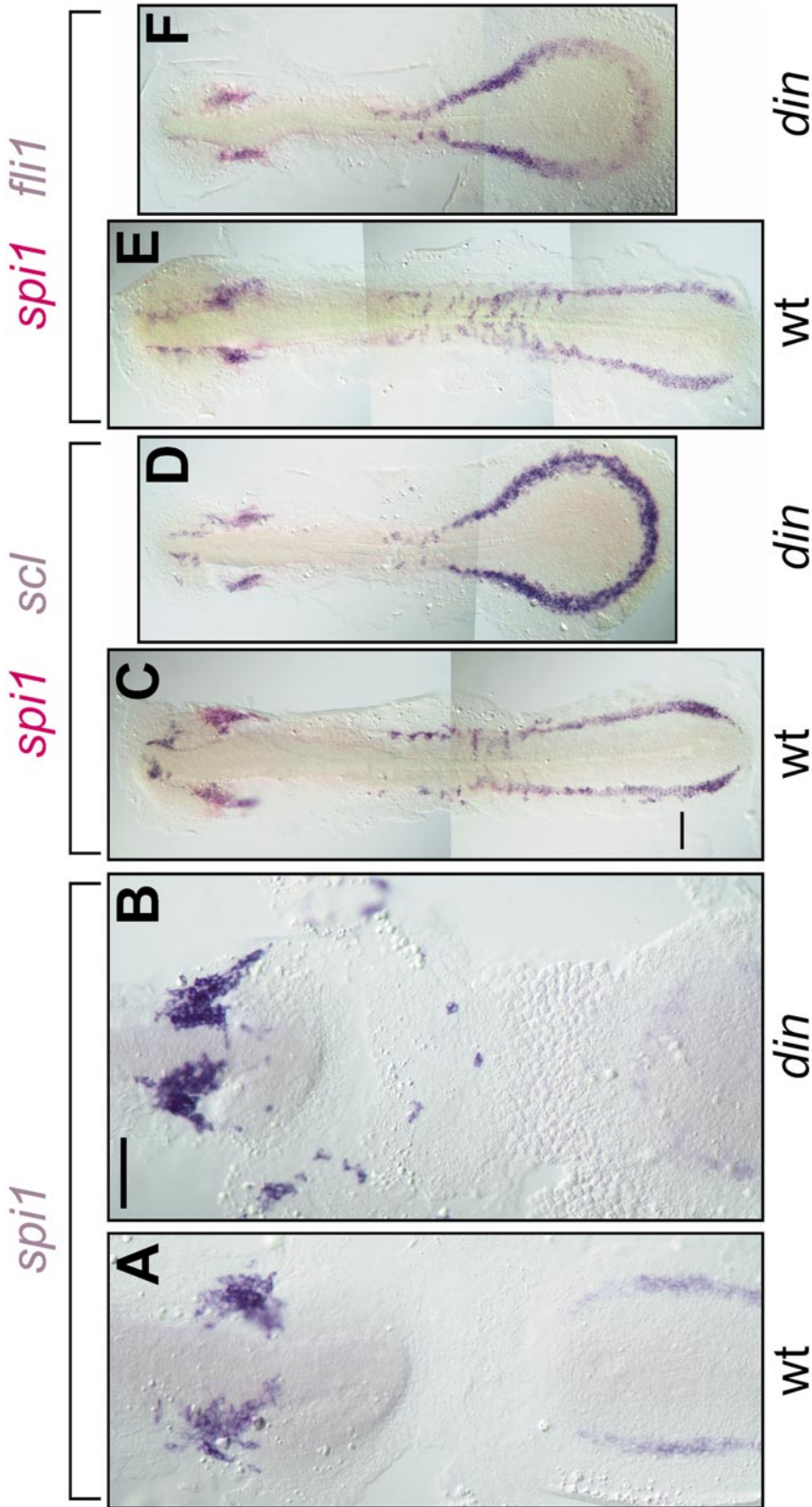
FIG. 9. Expression of spi1, fli1, and scl in wild-type and chordino (din) zebrafish embryos. (A, B) Flat-mount 12-somite wild-type (A) and chordino (B) embryos stained with spi1 riboprobe. Embryos were opened in the middle of their backs, deyolked, and flat mounted to display ventral views of the discontinuous rostral (top) and caudal (bottom) ends of the embryo. In chordino, the number of rostral spi1⁺ cells is not reduced, and they are more dispersed. (C–F) Wild-type (C, E) and chordino (D, F) embryos stained with scl (blue in C, D) or fli1 (blue in E, F) and spi1 (red in C–F) riboprobes. Although the rostral LPM is somewhat reduced in size in chordino, it still makes cell types expressing these three markers, while the caudal LPM is greatly enlarged. The extent of caudal of spi1-expression was not reduced in chordino mutants, although it was altered in shape; this domain of expression is more completely shown in (D) and (F), rather than in (B). Scale bars, 100 μm.
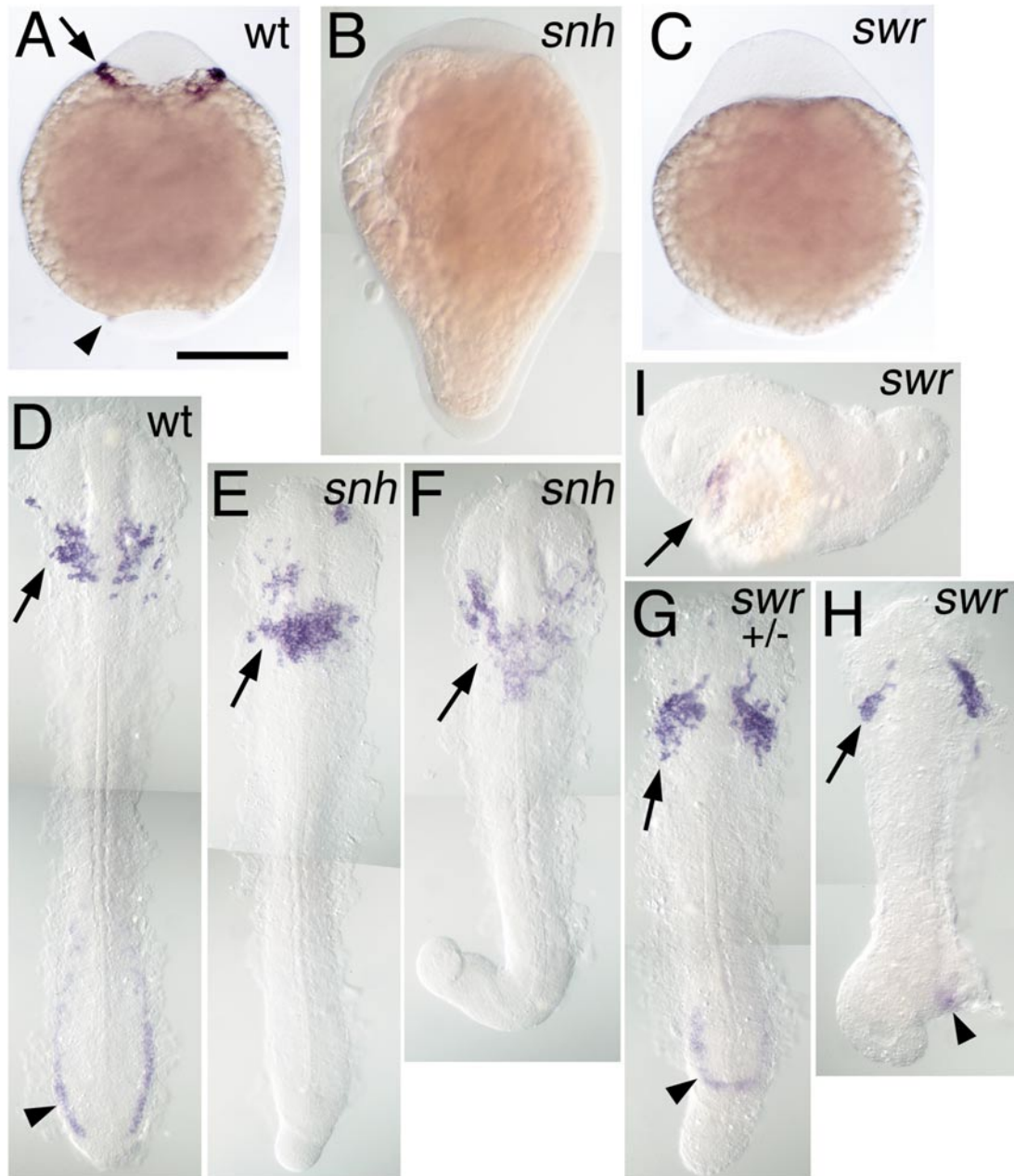
FIG. 10. Rostral expression of *spi1* in BMP pathway mutants. Expression of *spi1* is shown in the 8-somite stage (A–C) and 15-somite stage (D–I) embryos, in wt (A, D), *snailhouse/bmp7* (*snh*; B, E, F), and *swirl/bmp2b* (*swr*; B, G–I) loss-of-function genetic backgrounds. Both *snh* and *swr* phenotypes are variably expressive: (E, F) Increasingly severe *snh* homozygous recessive phenotypes; (G) a severe *swr* dominant heterozygotic phenotype; (H, I) Increasingly severe *swr* homozygote phenotypes. (A–C) Embryos in whole mount from a ventral view, anterior to the top. (D–H) Embryos dissected from yolk and flat mounted with anterior to the top; (I) A *swr* embryo in lateral view, anterior to the left. Rostral expression of *spi1* is marked with an arrow (A, D–I), and caudal expression is marked with an arrowhead (A, D, G, H), showing that despite the loss of the caudal domain, rostral *spi1* expression is maintained in embryos exhibiting extreme "dorsalization."

expression. This contrasts with our observations in zebrafish, where by *in situ* hybridization, *spi1* expression precedes *cfms* expression (G.J.L., unpublished data). However, it is possible that the failure to detect early *Spi-1* expression in the mouse whole-mount *in situ* hybridization preparations reflected the sensitivity of the technique, rather than the absolute absence of gene expression.

Taken collectively, although the evidence derives from different molecular markers in the different species mentioned above, these observations strongly suggest that a
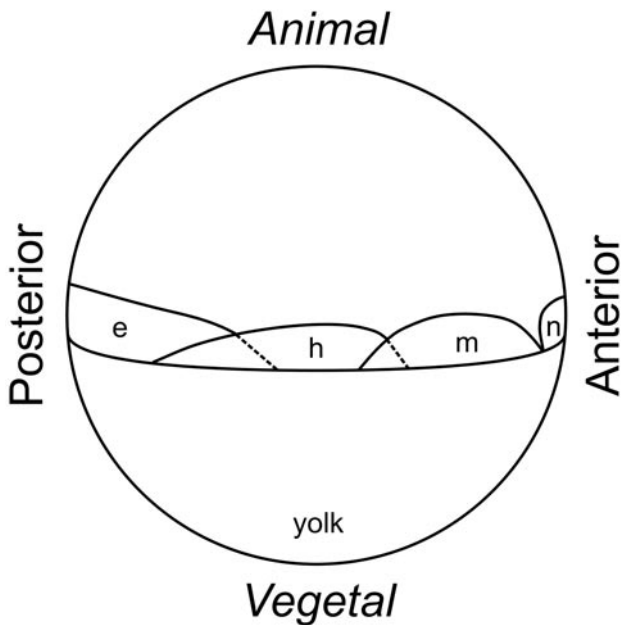
FIG. 11. Proposed fate map for ventral mesodermal tissues in the zebrafish gastrula. A representation of the zebrafish gastrula (shield stage, 6 hpf) based on the fate maps created by Kimmel *et al.* (1990) and Warga and Nusslein-Volhard (1999), indicating the proposed site of origin of the myeloid lineage (m) and its spatial relations to those of notochord (n), heart (h), and erythroid lineage (e).

focus of early myeloid commitment located immediately rostrally of the developing heart is not a unique feature of zebrafish development, but characterizes early myeloid development in other vertebrates as diverse as frogs and mammals.

A Revised Gastrula Fate Map for the Ventral Mesoderm in Zebrafish

In the current zebrafish fate map, hematopoietically fated precursor cells derive from a location in the gastrula opposite that of the future shield (Kimmel *et al.*, 1990; Warga and Nusslein-Volhard, 1999). We propose a refinement to the zebrafish fate map that separates these fates in the pregastrulation embryo (Fig. 11), and also suggest that this arrangement holds true for the early embryos of other vertebrates. We propose that in the zebrafish gastrula, cells destined for more rostral LPM positions (fated to become myeloid cells) are located near the margin and closer to the shield than the cells destined for caudal LPM locations (fated to become erythroid cells), and furthermore, that these two populations have cells of the heart field interposed between them (Stainier *et al.*, 1993). Through gastrulation, the myeloid and erythroid precursor cells locate to their respective rostral and caudal positions along the LPM, still separated by the cardiac anlage. Then after gastrulation, according to their rostrocaudal location, and possibly

now under local rather than programmed influences, these hematopoietically fated cells progress toward erythroid or myeloid outcomes. BMP signaling is required for both erythroid and myeloid outcomes, although at high levels it represses the latter. In contrast, *chordin* antagonizes the effect of BMP signaling, favoring a myeloid outcome in hematopoietically fated domains, although it itself is not directly required for a myeloid outcome.

Combining our observations with those made in other vertebrates mentioned above leads us to also propose a general model of early myeloid development in vertebrate embryos, in which the myeloid lineage arise from cells in the early embryo that are anatomically isolated from the erythroid lineage and adjacent to the heart anlage, and show a differential response to BMP signals from erythroid cells. These predictions now warrant evaluation in other vertebrate embryos.

Although the processes of erythropoiesis and myelopoiesis ultimately colocate in the adult, there seems to be no necessity to presume that they will be anatomically colocalized in the precirculation embryo. Although both cell types benefit from the mobility afforded by the circulation once it is established, in the precirculation embryo, there is little necessity that the system generating erythrocytes for oxygen transportation would necessarily be sited with that generating leukocytes for debris removal and front-of-the-line host defense. Indeed, in the early zebrafish embryo, the anatomical separation of these two developmental pathways has now been demonstrated.

ACKNOWLEDGMENTS

REFERENCES

Al-Adhami, M. A., and Kunz, Y. W. (1977). Ontogenesis of haematopoietic sites in *Brachydanio rerio* (Hamilton-Buchanan) (Teleostei). *Dev. Growth Differ.* **19,** 171–179.

Alexander, J., Stainier, D. T., and Yelon, D. (1998). Screening mosaic F1 females for mutations affecting zebrafish heart induction and patterning. *Dev. Genet.* **22,** 288–299.

Amatruda, J. F., and Zon, L. I. (1999). Dissecting hematopoiesis and disease using the zebrafish. *Dev. Biol.* **216,** 1–15.

Anderson, M. K., Sun, X., Miracle, A. L., Litman, G. W., and Rothenberg, E. V. (2001). Evolution of hematopoiesis: Three members of the PU.1 transcription factor family in a cartilaginous fish, *Raja eglantaria. Proc. Natl. Acad. Sci. USA* **98,** 553–558.

Bennett, C. M., Kanki, J. P., Rhodes, J., Liu, T. X., Paw, B. H., Kieran, M. W., Langenau, D. M., Delahaye-Brown, A., Zon, L. I., Fleming, M. D., and Look, A. T. (2001). Myelopoiesis in the zebrafish, *Danio rerio. Blood* **98,** 643–651.

Bertrand, C., Chatonnet, A., Takke, C., Yan, Y., Postlethwait, J., Toutant, J. P., and Cousin, X. (2001). Zebrafish acetylcholinesterase is encoded by a single gene localized on linkage group 7. Gene structure and polymorphism: Molecular forms and expression pattern during development. *J. Biol. Chem.* **276,** 464–474.

Blake, T., Adya, N., Kim, C. H., Oates, A. C., Zon, L., Chitnis, A., Weinstein, B. M., and Liu, P. P. (2000). Zebrafish homolog of the leukemia gene CBFB: its expression during embryogenesis and its relationship to scl and gata-1 in hematopoiesis. *Blood* **96,** 4178–4184.

Brownlie, A., Donovan, A., Pratt, S. J., Paw, B. H., Oates, A. C., Brugnara, C., Witkowska, H. E., Sassa, S., and Zon, L. I. (1998). Positional cloning of the zebrafish sauternes gene: A model for congenital sideroblastic anaemia. *Nat. Genet.* **20,** 244–250.

Chan, F. Y., Robinson, J., Brownlie, A., Shivdasani, R. A., Donovan, A., Brugnara, C., Kim, J., Lau, B. C., Witkowska, H. E., and Zon, L. I. (1997). Characterization of adult alpha- and beta-globin genes in the zebrafish. *Blood* **89,** 688–700.

Childs, S., Weinstein, B. M., Mohideen, M. A., Donohue, S., Bonkovsky, H., and Fishman, M. C. (2000). Zebrafish dracula encodes ferrochelatase and its mutation provides a model for erythropoietic protoporphyria. *Curr. Biol.* **10,** 1001–1004.

Conway, G., Margoliath, A., Wong-Madden, S., Roberts, R. J., and Gilbert, W. (1997). Jak1 kinase is required for cell migrations and anterior specification in zebrafish embryos. *Proc. Natl. Acad. Sci. USA* **94,** 3082–3087.

Dale, L., Howes, G., Price, B. M., and Smith, J. C. (1992). Bone morphogenetic protein 4: A ventralizing factor in early Xenopus development. *Development* **115,** 573–585.

Detrich, H. W., Kieran, M. W., Chan, F. Y., Barone, L. M., Yee, K., Rundstadler, J. A., Pratt, S., Ransom, D., and Zon, L. I. (1995). Intraembryonic hematopoietic cell migration during vertebrate development. *Proc. Natl. Acad. Sci. USA* **92,** 10713–10717.

Dick, A., Hild, M., Bauer, H., Imai, Y., Maifeld, H., Schier, A. F., Talbot, W. S., Bouwmeester, T., and Hammerschmidt, M. (2000). Essential role of Bmp7 (snailhouse) and its prodomain in dorsoventral patterning of the zebrafish embryo. *Development* **127,** 343–354.

Donovan, A., Brownlie, A., Zhou, Y., Shepard, J., Pratt, S. P., Moynihan, J., Paw, B. H., Drejer, A., Barut, B., Zapata, A., Law, T. C., Brugnara, C., Lux, S. E., Pinkus, G. S., Pinkus, J. L., Kingsley, P. D., Palis, J., Fleming, M. D., Andrews, N. C., and Zon, L. I. (2000). Positional cloning of zebrafish ferroportin1 identifies a conserved vertebrate iron exporter. *Nature* **403,** 776–781.

Gering, M., Rodaway, A. R., Gottgens, B., Patient, R. K., and Green, A. R. (1998). The SCL gene specifies haemangioblast development from early mesoderm. *EMBO J.* **17,** 4029–4045.

Griffin, K. J., Amacher, S. L., Kimmel, C. B., and Kimelman, D. (1998). Molecular identification of spadetail: Regulation of zebrafish trunk and tail mesoderm formation by T-box genes. *Development* **125,** 3379–3388.

Haire, R. N., Miracle, A. L., Rast, J. P., and Litman, G. W. (2000). Members of the Ikaros gene family are present in early representative vertebrates. *J. Immunol.* **165,** 306–312.

Hammerschmidt, M., Pelegri, F., Mullins, M. C., Kane, D. A., van Eeden, F. J., Granato, M., Brand, M., Furutani-Seiki, M., Haffter, P., Heisenberg, C. P., Jiang, Y. J., Kelsh, R. N., Odenthal, J., Warga, R. M., and Nusslein-Volhard, C. (1996a). dino and mercedes, two genes regulating dorsal development in the zebrafish embryo. *Development* **123,** 95–102.

Hammerschmidt, M., Serbedzija, G. N., and McMahon, A. P. (1996b). Genetic analysis of dorsoventral pattern formation in the zebrafish: Requirement of a BMP-like ventralizing activity and its dorsal repressor. *Genes Dev.* **10,** 2452–2461.

Hauptmann, G., and Gerster, T. (1994). Two-color whole-mount in situ hybridization to vertebrate and Drosophila embryos. *Trends Genet.* **10,** 266.

Herbomel, P., Thisse, B., and Thisse, C. (1999). Ontogeny and behaviour of early macrophages in the zebrafish embryo. *Development* **126,** 3735–3745.

Jones, C. M., Lyons, K. M., Lapan, P. M., Wright, C. V., and Hogan, B. L. (1992). DVR-4 (bone morphogenetic protein-4) as a posterior-ventralizing factor in Xenopus mesoderm induction. *Development* **115,** 639–647.

Kataoka, H., Ochi, M., Enomoto, K., and Yamaguchi, A. (2000). Cloning and embryonic expression patterns of the zebrafish runt domain genes, runxa and runxb. *Mech. Dev.* **98,** 139–143.

Kimmel, C. B., Kane, D. A., Walker, C., Warga, R. M., and Rothman, M. B. (1989). A mutation that changes cell movement and cell fate in the zebrafish embryo. *Nature* **337,** 358–362.

Kimmel, C. B., Warga, R. M., and Schilling, T. F. (1990). Origin and organization of the zebrafish fate map. *Development* **108,** 581–594.

Kishimoto, Y., Lee, K. H., Zon, L., Hammerschmidt, M., and Schulte-Merker, S. (1997). The molecular nature of zebrafish swirl: BMP2 function is essential during early dorsoventral patterning. *Development* **124,** 4457–4466.

Klemsz, M. J., and Maki, R. A. (1996). Activation of transcription by PU.1 requires both acidic and glutamine domains. *Mol. Cell. Biol.* **16,** 390–397.

Kozlowski, D. J., Murakami, T., Ho, R. K., and Weinberg, E. S. (1997). Regional cell movement and tissue patterning in the zebrafish embryo revealed by fate mapping with caged fluorescein. *Biochem. Cell Biol.* **75,** 551–562.

Lane, M. C., and Sheets, M. D. (2000). Designation of the anterior/posterior axis in pregastrula *Xenopus laevis. Dev. Biol.* **225,** 37–58.

Lane, M. C., and Smith, W. C. (1999). The origins of primitive blood in Xenopus: Implications for axial patterning. *Development* **126,** 423–434.

Lee, K. H., Marden, J. J., Thompson, M. S., MacLennan, H., Kishimoto, Y., Pratt, S. J., Schulte-Merker, S., Hammerschmidt, M., Johnson, S. L., Postlethwaite, J. H., Beier, D. C., and Zon, L. I. (1998). Cloning and genetic mapping of zebrafish BMP-2. *Dev. Genet.* **23,** 97–103.

Liao, E. C., Paw, B. H., Oates, A. C., Pratt, S. J., Postlethwait, J. H., and Zon, L. I. (1998). SCL/Tal-1 transcription factor acts downstream of cloche to specify hematopoietic and vascular progenitors in zebrafish. *Genes Dev.* **12,** 621–626.

Liao, E. C., Paw, B. H., Peters, L. L., Zapata, A., Pratt, S. J., Do, C. P., Lieschke, G., and Zon, L. I. (2000a). Hereditary spherocytosis in zebrafish riesling illustrates evolution of erythroid β-spectrin structure, and function in red cell morphogenesis and membrane stability. *Development* **127,** 5123–5132.

Liao, W., Ho, C., Yan, Y. L., Postlethwait, J., and Stainier, D. Y. (2000b). Hhex and scl function in parallel to regulate early endothelial and blood differentiation in zebrafish. *Development* **127,** 4303–4313.

Lichanska, A. M., Browne, C. M., Henkel, G. W., Murphy, K. M., Ostrowski, M. C., McKercher, S. R., Maki, R. A., and Hume, D. A. (1999). Differentiation of the mononuclear phagocyte system during mouse embryogenesis: The role of transcription factor PU.1. *Blood* **94,** 127–138.

Lieschke, G. J., Oates, A. C., Crowhurst, M. O., Ward, A. C., and Layton, J. E. (2001). Morphological and functional characterization of granulocytes and macrophages in embryonic and adult zebrafish. *Blood* **98,** 3087–3096.

Lyons, S. E., Shue, B. C., Oates, A. C., Zon, L. I., and Liu, P. P. (2001). A novel myeloid-restricted zebrafish CCAAT/enhancer-binding protein with a potent transcriptional activation domain. *Blood* **97,** 2611–2617.

Maeno, M., Mead, P. E., Kelley, C., Xu, R., Kung, H., Suzuki, A., Ueno, N., and Zon, L. I. (1996). The role of BMP-4 and GATA-2 in the induction and differentiation of hematopoietic mesoderm in *Xenopus laevis*. *Blood* **88,** 1965–1972.

Martinez-Barbera, J. P., Toresson, H., Da Rocha, S., and Krauss, S. (1997). Cloning and expression of three members of the zebrafish Bmp family: Bmp2a, Bmp2b and Bmp4. *Gene* **198,** 53–59.

Marvin, M. J., Di Rocco, G., Gardiner, A., Bush, S. M., and Lassar, A. B. (2001). Inhibition of Wnt activity induces heart formation from posterior mesoderm. *Genes Dev.* **15,** 316–327.

McKercher, S. R., Torbett, B. E., Anderson, K. L., Henkel, G. W., Vestal, D. J., Baribault, H., Klemsz, M., Feeney, A. J., Wu, G. E., Paige, C. J., and Maki, R. A. (1996). Targeted disruption of the PU.1 gene results in multiple hematopoietic abnormalities. *EMBO J.* **15,** 5647–5658.

Miller-Bertoglio, V. E., Fisher, S., Sanchez, A., Mullins, M. C., and Halpern, M. E. (1997). Differential regulation of chordin expression in mutant zebrafish. *Dev. Biol.* **192,** 537–550.

Miller-Bertoglio, V., Carmany-Rampey, A., Furthauer, M., Gonzalez, E. M., Thisse, C., Thisse, B., Halpern, M. E., and Solnica-Krezel, L. (1999). Maternal and zygotic activity of the zebrafish ogon locus antagonizes BMP signaling. *Dev. Biol.* **214,** 72–86.

Miyanaga, Y., Shiurba, R., Nagata, S., Pfeiffer, C. J., and Asashima, M. (1998). Induction of blood cells in Xenopus embryo explants. *Dev. Genes Evol.* **207,** 417–426.

Moorman, S. J. (2001). Anatomical nomenclature for zebrafish. *Zebrafish Science Monitor*, 7–8.

Moreau-Gachelin, F., Ray, D., Mattei, M. G., Tambourin, P., and Tavitian, A. (1989). The putative oncogene Spi-1: Murine chromosomal localization and transcriptional activation in murine acute erythroleukemias. *Oncogene* **4,** 1449–1456.

Morris, L., Graham, C. F., and Gordon, S. (1991). Macrophages in haemopoietic and other tissues of the developing mouse detected by the monoclonal antibody F4/80. *Development* **112,** 517–526.

Mullins, M. C., Hammerschmidt, M., Kane, D. A., Odenthal, J., Brand, M., van Eeden, F. J., Furutani-Seiki, M., Granato, M., Haffter, P., Heisenberg, C. P., Jiang, Y. J., Kelsh, R. N., and Nusslein-Volhard, C. (1996). Genes establishing dorsoventral pattern formation in the zebrafish embryo: The ventral specifying genes. *Development* **123,** 81–93.

Neave, B., Holder, N., and Patient, R. (1997). A graded response to BMP-4 spatially coordinates patterning of the mesoderm and ectoderm in the zebrafish. *Mech. Dev.* **62,** 183–195.

Nikaido, M., Tada, M., Saji, T., and Ueno, N. (1997). Conservation of BMP signaling in zebrafish mesoderm patterning. *Mech. Dev.* **61,** 75–88.

Oates, A. C., Brownlie, A., Pratt, S. J., Irvine, D. V., Liao, E. C., Paw, B. H., Dorian, K. J., Johnson, S. L., Postlethwait, J. H., Zon, L. I., and Wilks, A. F. (1999a). Gene duplication of zebrafish JAK2 homologs is accompanied by divergent embryonic expression patterns: Only jak2a is expressed during erythropoiesis. *Blood* **94,** 2622–2636.

Oates, A. C., Wollberg, P., Pratt, S. J., Paw, B. H., Johnson, S. L., Ho, R. K., Postlethwait, J. H., Zon, L. I., and Wilks, A. F. (1999b). Zebrafish stat3 is expressed in restricted tissues during embryogenesis and stat1 rescues cytokine signaling in a STAT1-deficient human cell line. *Dev. Dyn.* **215,** 352–370.

Ohinata, H., Tochinai, S., and Katagiri, C. (1990). Occurrence of nonlymphoid leukocytes that are not derived from blood islands in *Xenopus laevis* larvae. *Dev. Biol.* **141,** 123–129.

Parichy, D. M., Ransom, D. G., Paw, B., Zon, L. I., and Johnson, S. L. (2000). An orthologue of the kit-related gene fms is required for development of neural crest-derived xanthophores and a subpopulation of adult melanocytes in the zebrafish, *Danio rerio*. *Development* **127,** 3031–3044.

Piccolo, S., Sasai, Y., Lu, B., and De Robertis, E. M. (1996). Dorsoventral patterning in Xenopus: Inhibition of ventral signals by direct binding of chordin to BMP-4. *Cell* **86,** 589–598.

Pongubala, J. M., Van Beveren, C., Nagulapalli, S., Klemsz, M. J., McKercher, S. R., Maki, R. A., and Atchison, M. L. (1993). Effect of PU.1 phosphorylation on interaction with NF-EM5 and transcriptional activation. *Science* **259,** 1622–1625.

Prince, V. E., Moens, C. B., Kimmel, C. B., and Ho, R. K. (1998). Zebrafish hox genes: Expression in the hindbrain region of wild-type and mutants of the segmentation gene, valentino. *Development* **125,** 393–406.

Ransom, D. G., Haffter, P., Odenthal, J., Brownlie, A., Vogelsang, E., Kelsh, R. N., Brand, M., van Eeden, F. J., Furutani-Seiki, M., Granato, M., Hammerschmidt, M., Heisenberg, C. P., Jiang, Y. J., Kane, D. A., Mullins, M. C., and Nusslein-Volhard, C. (1996). Characterization of zebrafish mutants with defects in embryonic hematopoiesis. *Development* **123,** 311–319.

Rekhtman, N., Radparvar, F., Evans, T., and Skoultchi, A. I. (1999). Direct interaction of hematopoietic transcription factors PU.1 and GATA-1: Functional antagonism in erythroid cells. *Genes Dev.* **13,** 1398–1411.

Ruvinsky, I., Silver, L. M., and Ho, R. K. (1998). Characterization of the zebrafish tbx16 gene and evolution of the vertebrate T-box family. *Dev. Genes Evol.* **208,** 94–99.

Sasai, Y., Lu, B., Steinbeisser, H., Geissert, D., Gont, L. K., and De Robertis, E. M. (1994). Xenopus chordin: A novel dorsalizing factor activated by organizer-specific homeobox genes. *Cell* **79,** 779–790.

Schneider, V. A., and Mercola, M. (2001). Wnt antagonism initiates cardiogenesis in *Xenopus laevis*. *Genes Dev.* **15,** 304–315.

Schulte-Merker, S., Ho, R. K., Herrmann, B. G., and Nusslein-Volhard, C. (1992). The protein product of the zebrafish homologue of the mouse T gene is expressed in nuclei of the germ ring and the notochord of the early embryo. *Development* **116,** 1021–1032.

Schulte-Merker, S., Lee, K. J., McMahon, A. P., and Hammerschmidt, M. (1997). The zebrafish organizer requires chordino. *Nature* **387,** 862–863.

Scott, E. W., Simon, M. C., Anastasi, J., and Singh, H. (1994). Requirement of transcription factor PU.1 in the development of multiple hematopoietic lineages. *Science* **265,** 1573–1577.

Sharrocks, A. D., Brown, A. L., Ling, Y., and Yates, P. R. (1997). The ETS-domain transcription factor family. *Int. J. Biochem. Cell Biol.* **29,** 1371–1387.

Shepard, J. L., and Zon, L. I. (2000). Developmental derivation of embryonic and adult macrophages. *Curr. Opin. Hematol.* **7,** 3–8.

Shintani, S., Terzic, J., Sato, A., Saraga-Babic, M., O'hUigin, C., Tichy, H., and Klein, J. (2000). Do lampreys have lymphocytes? The Spi evidence. *Proc. Natl. Acad. Sci. USA* **97,** 7417–7422.

Stainier, D. Y., Lee, R. K., and Fishman, M. C. (1993). Cardiovascular development in the zebrafish. I. Myocardial fate map and heart tube formation. *Development* **119,** 31–40.

Stanley, E., Lieschke, G. J., Grail, D., Metcalf, D., Hodgson, G., Gall, J. A., Maher, D. W., Cebon, J., Sinickas, V., and Dunn, A. R. (1994). Granulocyte/macrophage colony-stimulating factor-deficient mice show no major perturbation of hematopoiesis but develop a characteristic pulmonary pathology. *Proc. Natl. Acad. Sci. USA* **91,** 5592–5596.

Thompson, J. D., Gibson, T. J., Plewniak, F., Jeanmougin, F., and Higgins, D. G. (1997). The CLUSTAL X windows interface: Flexible strategies for multiple sequence alignment aided by quality analysis tools. *Nucleic Acids Res.* **25,** 4876–4882.

Thompson, M. A., Ransom, D. G., Pratt, S. J., MacLennan, H., Kieran, M. W., Detrich, H. W., Vail, B., Huber, T. L., Paw, B., Brownlie, A. J., Oates, A. C., Fritz, A., Gates, M. A., Amores, A., Bahary, N., Talbot, W. S., Her, H., Beier, D. R., Postlethwait, J. H., and Zon, L. I. (1998). The cloche and spadetail genes differentially affect hematopoiesis and vasculogenesis. *Dev. Biol.* **197,** 248–269.

Tracey, W. D., Pepling, M. E., Horb, M. E., Thomsen, G. H., and Gergen, J. P. (1998). A Xenopus homologue of aml-1 reveals unexpected patterning mechanisms leading to the formation of embryonic blood. *Development* **125,** 1371–1380.

Tzahor, E., and Lassar, A. B. (2001). Wnt signals from the neural tube block ectopic cardiogenesis. *Genes Dev.* **15,** 255–260.

Wang, H., Long, Q., Marty, S. D., Sassa, S., and Lin, S. (1998). A zebrafish model for hepatoerythropoietic porphyria. *Nat. Genet.* **20,** 239–243.

Warga, M. W., and Nusslein-Volhard, C. (1999). Origin and development of the zebrafish endoderm. *Development* **126,** 827–838.

Weinstein, B. M., Schier, A. F., Abdelilah, S., Malicki, J., Solnica-Krezel, L., Stemple, D. L., Stainier, D. Y., Zwartkruis, F., Driever, W., and Fishman, M. C. (1996). Hematopoietic mutations in the zebrafish. *Development* **123,** 303–309.

Willett, C. E., Zapata, A. G., Hopkins, N., and Steiner, L. A. (1997). Expression of zebrafish rag genes during early development identifies the thymus. *Dev. Biol.* **182,** 331–341.

Wilson, E. T., Cretekos, C. J., and Helde, K. A. (1995). Cell mixing during early epiboly in the zebrafish embryo. *Dev. Genet.* **17,** 6–15.

Yoder, J. A., and Litman, G. W. (2000). The zebrafish fth1, slc3a2, men1, pc, fgf3 and cycd1 genes define two regions of conserved synteny between linkage group 7 and human chromosome 11q13. *Gene* **261,** 235–242.

Zhang, P., Zhang, X., Iwama, A., Yu, C., Smith, K. A., Mueller, B. U., Narravula, S., Torbett, B. E., Orkin, S. H., and Tenen, D. G. (2000). PU.1 inhibits GATA-1 function and erythroid differentiation by blocking GATA-1 DNA binding. *Blood* **96,** 2641–2648.